ARL-TR-9686 • MAY 2023

DEVCOM ARMY RESEARCH LABORATORY

A Large Deformation Multiphase Continuum Mechanics Model for Shock Loading of Lung Parenchyma. Part I: Theory

by Zachariah T Irwin, Richard A Regueiro, and John D Clayton

NOTICES

Disclaimers

The findings in this report are not to be construed as an official Department of the Army position unless so designated by other authorized documents.

Citation of manufacturer's or trade names does not constitute an official endorsement or approval of the use thereof.

Destroy this report when it is no longer needed. Do not return it to the originator.

ARL-TR-9686 ● MAY 2023

A Large Deformation Multiphase Continuum Mechanics Model for Shock Loading of Lung Parenchyma. Part I: Theory

Zachariah T Irwin
University of Colorado, Boulder

Richard A Regueiro and John D Clayton
DEVCOM Army Research Laboratory

REPORT DOCUMENTATION PAGE

Form Approved
OMB No. 0704-0188

1. REPORT DATE *(DD-MM-YYYY)*	2. REPORT TYPE	3. DATES COVERED (From - To)
May 2023	Technical Report	January 2022–March 2023

4. TITLE AND SUBTITLE
A Large Deformation Multiphase Continuum Mechanics Model for Shock Loading of Lung Parenchyma. Part I: Theory

5a. CONTRACT NUMBER

5b. GRANT NUMBER

5c. PROGRAM ELEMENT NUMBER

6. AUTHOR(S)
Zachariah T Irwin, Richard A Regueiro, and John D Clayton

5d. PROJECT NUMBER

5e. TASK NUMBER

5f. WORK UNIT NUMBER

7. PERFORMING ORGANIZATION NAME(S) AND ADDRESS(ES)
DEVCOM Army Research Laboratory
ATTN: FCDD-RLA-TB
Aberdeen Proving Ground, MD 21005-5066

8. PERFORMING ORGANIZATION REPORT NUMBER
ARL-TR-9686

9. SPONSORING/MONITORING AGENCY NAME(S) AND ADDRESS(ES)

10. SPONSOR/MONITOR'S ACRONYM(S)

11. SPONSOR/MONITOR'S REPORT NUMBER(S)

12. DISTRIBUTION/AVAILABILITY STATEMENT
Approved for public release; distribution is unlimited.

13. SUPPLEMENTARY NOTES
ORCID ID: John Clayton, 0000-0003-4107-6282

14. ABSTRACT
A finite-strain theory of a biphasic mixture, with coupled pore fluid flow and solid skeleton deformation, of a soft porous material has been developed for high strain-rate dynamic loading. The constitutive model is nonlinear elastic and accounts for the compressibility of the pore air. The formulation does not require equivalency of acceleration of pore fluid to that of solid skeleton, but rather allows them to be different. Through implementation of the concept of solid extra stress, the theory is able to distinguish among solid skeleton, pore fluid (air), and total pressures, and similarly among stress tensors for each constituent. General features of the constitutive description are specialized for an application to shock loading of lung parenchyma. This is the first in a series of three reports.

15. SUBJECT TERMS
theory of porous media, soft tissue mechanics, shock waves, lung, Sciences of Extreme Materials, Terminal Effects

16. SECURITY CLASSIFICATION OF:			17. LIMITATION OF ABSTRACT	18. NUMBER OF PAGES	19a. NAME OF RESPONSIBLE PERSON
a. REPORT	b. ABSTRACT	c. THIS PAGE			John D Clayton
Unclassified	Unclassified	Unclassified	UU	63	19b. TELEPHONE NUMBER (Include area code) 410-278-6146

Contents

List of Figures

Acknowledgments

The authors acknowledge support from the Army Research Directorate of the US Army Combat Capabilities Development Command (DEVCOM) Army Research Laboratory (ARL). R Regueiro acknowledges support from a Joint Faculty Appointment at ARL. Z Irwin acknowledges the Department of Defense SMART scholarship program for doctoral students. This work utilized resources from the University of Colorado Boulder Research Computing Group, which is supported by the National Science Foundation (awards ACI-1532235 and ACI-1532236), the University of Colorado Boulder, and Colorado State University. This work was supported in part by high-performance computer time and resources from the DoD High Performance Computing Modernization Program.

This report encompasses and extends research recently submitted in abbreviated form by the authors in a refereed article* to the *International Journal for Numerical Methods in Engineering* (2023).

*Irwin Z, Clayton J, Regueiro R. A large deformation multiphase continuum mechanics model for shock loading of soft porous materials. International Journal for Numerical Methods in Engineering. Forthcoming 2023.

1. Introduction

1.1 Background

Shock waves induce large pressure gradients, which are assumed to directly cause microstructural tearing of the lung parenchyma leading to hemorrhaging.[1–3] Broadly speaking, injury pathology and progression are well understood[4]; however the details of how injury propagates through the lung parenchyma at the ultrastructural (tissue fibers) and microstructural (air sac) level are not well understood and are an active area of research.[5–8] The approach undertaken by Freed et al.[7] to model the microstructural level necessitates a multiscale model of the whole lung tissue, which includes the highly heterogeneous structure of the lung parenchyma as seen from the microstructure in Fig. 1.

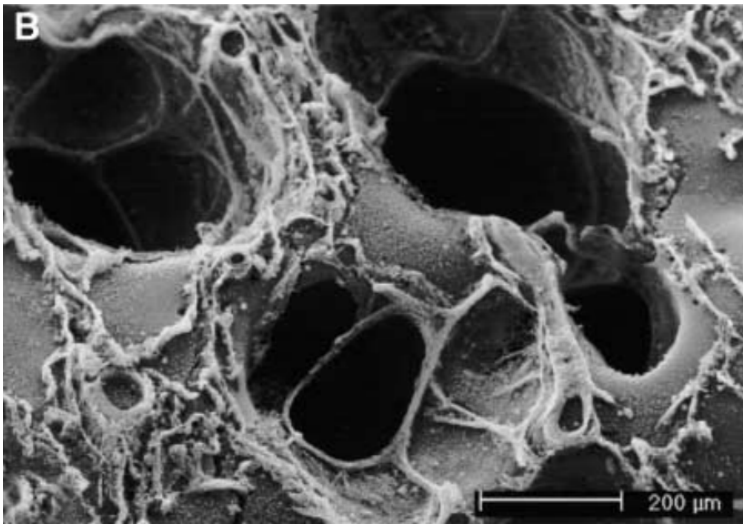

Fig. 1 Scanning electron micrograph of intact alveolar air sacs, adapted from Tsokos et al.[3]

The lung parenchyma is comprised of alveolar air sacs ranging from 100 to 330 µm in diameter[9] and connective tissues made up of a complex network of collagen and elastin fibers.[10] Collagen fibers in the parenchyma organize to form both an axial fiber network that connects the central airways to the alveolar ducts and a network that extends from the visceral pleura of the lung to the alveolar ducts. The elastin fibers are connected to the collagen fibers via microfibrils and proteoglycans, the latter which have chemical interactions in addition to topological interactions with

the collagen fibrils. The composition and physical dimensions of these unique collagen fibers play a great role in determining the stiffness of these networks. Furthermore, mechanical forces that act upon the extra-cellular matrix (ECM), in which the collagen and elastin fibers reside, can induce the secretion of growth factors that accelerate ECM remodeling and alter the microstructural composition of the collagen and elastin networks.[10]

At low strain, the stress response of fibril network appears to be heterogeneous as the elastin fibers bear much of the stress. However, at higher rates of strain, such as those induced by a shock wave, elastin fibers are prone to rupture[7] and the remaining stress response percolates through the collagen fibril networks as the collagen fibers start to extend to their uncoiled lengths. This increases the stress response of the entire lung parenchyma.[11] Bronchiole tubes also affect load distribution in the impacted lung.[8] The complex roles that collagen and elastin fibers play in the dynamics of the lung parenchyma are beyond the scope of this report. These details are discussed by Freed et al.[7]; here we focus on the role that poro-elasto-dynamics plays at the mesoscopic level. Findings can be used to inform macroscopic, single-phase models of the lung for 3-D modeling of much larger domains.[5,6,12–15]

1.2 Approach

Mixture theory was first established at finite strain by Truesdell and Toupin.[16] More recent works include those by Bowen[17–19] and others[20–23] for mixture theory applied to porous media. Shock waves in mixtures were analyzed by Bowen and Wright.[24,25] The theory of porous media (TPM) is an appropriate approximation to a more robust, but much more computationally expensive, fluid-structure interaction (FSI) model at the pore length scale. In TPM, these interactions are smeared across a continuum material point, thereby simplifying not just the discretization of the governing mathematical equations (namely, mass balance, momentum balance, energy balance, and entropy inequality), but also the discretization of the geometry itself.

Lung parenchyma is a highly complex, heterogeneous material: refer to scanning electron microscope images in Tsokos et al.[3] Resolution would require representation by a detailed 3-D finite-element (FE) mesh to model the *explicit* FSI via, for example, coupled computational fluid dynamics-computational solid mechanics with arbitrary Lagrangian-Eulerian FE modeling. Such a framework would, in addition to being costly both to run the simulation and for mesh generation, be biased

toward the structure of the FE mesh. As such, work is needed to first accurately simulate the deformation of lung parenchyma using a multiphysics approach, before addressing damage and injury pathology at the microscale (i.e., alveolar regime) and linking that to the mesoscale (i.e., parenchymal regime). Here we incorporate TPM to take into account the different response times of the two constituents in the lung parenchyma subjected to shock loading: solid skeleton (s) (lung parenchyma) and the pore fluid (f) (air) that occupies the pore space.

Past numerical models involving TPM have typically addressed geological and geotechnical engineering applications (e.g., soil consolidation problems) wherein inertial terms are typically ignored, the solid and pore fluid constituents are nearly incompressible, and strains are small.[26,27] In other works,[28–31] inertial terms are retained, but small-strain theory is still assumed. In Li et al., Gajo and Denzer, and Regueiro et al.,[32–34] inertial terms are retained, constituents are compressible, nonlinear constitutive theory is present, and deformation is finite. However, in Li et al. and Regueiro et al.,[32,34] it was assumed that dynamic loading frequencies were relatively small ($\mathcal{O}(10^1\text{-}10^2)$ rad/s), and therefore the acceleration of the fluid phase was approximately the same as that of the solid phase, that is, $\boldsymbol{a}_{\mathrm{f}} \approx \boldsymbol{a}_{\mathrm{s}} = \boldsymbol{a}$. In this work, we continue from Regueiro et al.[34] but with the assumption that for higher-strain rate loadings, $\boldsymbol{a}_{\mathrm{f}} \neq \boldsymbol{a}_{\mathrm{s}}$, necessitating a "three-field" formulation,[34] and comparison to "two-field" formulation results. The three-field formulation is not new, see Zienkiewicz and Shiomi[35] for the initial theory and others[36–41] for various numerical implementations. However, to the best of our knowledge, no other authors have considered the following physics simultaneously: large deformations,[32–34,38,42–56] inertial effects,[28,29,31–34,36,38,41,43–45,48–50,52–59] nonlinearity of constitutive theory for the phases,[28,34,37,42,44–48,50,52–55,57] finitely compressible constituents,[28,29,33,34,41,43,50,54,58,60] and high strain-rate loading with nonlinear geometric effects.

Furthermore, many works in TPM use implicit time-stepping methods (e.g., the well-known Newmark-beta schemes) or semi-implicit time-stepping methods (e.g., Zienkiewicz et al.[30] and others[28,29,41]) which, even for dynamic loadings, are not always suitable computationally for shock loadings[61,62] wherein small time steps are required to resolve the shock physics. Those that do present explicit time integration schemes generally stick to the well-known central-difference scheme or variations thereof.[52,56] In subsequent work by the current authors, various choices of explicit

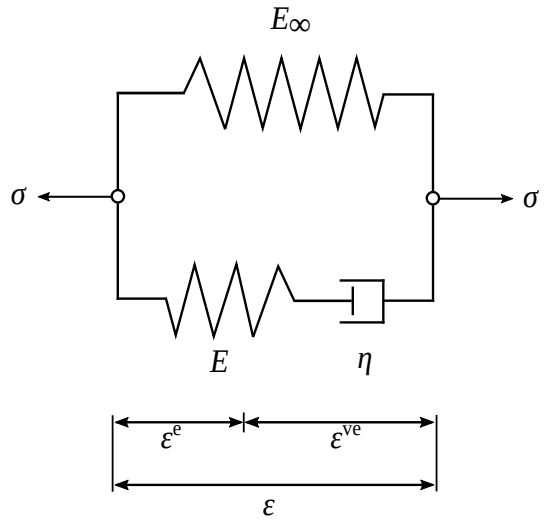

Fig. 2 The standard linear solid model, adapted from Simo and Hughes[63]

time integration schemes are presented and compared.

To help argue for the necessity of poromechanics models in this area of research (i.e., porous biological tissues), we briefly compare the stress relaxation times between a purely viscoelastic model and a poroelastic model at small strain. Comparisons are furnished in the remainder of Section 1.2.

1.2.1 Linear Viscoelasticity in One Dimension at Small Strain

Consider the following viscoelastic standard linear solid model of Fig. 2 with axial strain ϵ that can be decomposed into its elastic strain ϵ^e and viscoelastic strain ϵ^{ve} components. Then the total stress contributed by the two parallel elements of the model can be expressed as

$$\sigma = E_\infty \epsilon + \sigma^v \tag{1}$$

where E_∞ is the steady-state elastic modulus and

$$\sigma^v = \eta \dot{\epsilon}^{ve} = E\epsilon^e = E(\epsilon - \epsilon^{ve}) \tag{2}$$

where η is the viscosity of the dashpot. Rearranging Eq. 2 leads to the following ordinary differential equation (ODE):

$$\dot{\epsilon}^{ve} + \frac{1}{\tau}\epsilon^{ve} = \frac{1}{\tau}\epsilon \tag{3}$$

where $\tau = \eta/E$ is the time relaxation constant. We will solve for $\epsilon^{ve}(t)$ using the integration factor $\exp[t/\tau]$ and convolution integral as follows:

$$\begin{aligned}
&\exp[t/\tau]\dot{\epsilon}^{ve} + \frac{1}{\tau}\exp[t/\tau]\epsilon^{ve} = \frac{1}{\tau}\exp[t/\tau]\epsilon, \\
&\Rightarrow \int_{-\infty}^{t} \frac{d}{ds}\left(\exp[s/\tau]\epsilon^{ve}(s)\right) ds = \int_{-\infty}^{t} \frac{1}{\tau}\exp[s/\tau]\epsilon(s)\, ds, \\
&\Rightarrow \exp[t/\tau]\epsilon^{ve}(t) = \frac{1}{\tau}\int_{-\infty}^{t} \exp[s/\tau]\epsilon(s)\, ds, \\
&\Rightarrow \epsilon^{ve}(t) = \int_{-\infty}^{t} \frac{1}{\tau}\exp\left[(s-t)/\tau\right]\epsilon(s)\, ds; \\
&\frac{d}{ds}\left(\exp\left[(s-t)/\tau\right]\epsilon(s)\right) = \frac{1}{\tau}\exp\left[(s-t)/\tau\right]\epsilon(s) + \exp\left[(s-t)/\tau\right]\dot{\epsilon}(s), \\
&\Rightarrow \epsilon^{ve}(t) = \underbrace{\int_{-\infty}^{t} \frac{d}{ds}\left(\exp\left[(s-t)/\tau\right]\epsilon(s)\right) ds}_{:=\epsilon(t)} - \int_{-\infty}^{t} \exp\left[(s-t)/\tau\right]\dot{\epsilon}(s)\, ds
\end{aligned} \tag{4}$$

Thus the total stress may be written as follows:

$$\sigma(t) = E_\infty\epsilon(t) + E\int_{-\infty}^{t} \exp\left[(s-t)/\tau\right]\dot{\epsilon}(s)\, ds = \int_{-\infty}^{t} G(t-s)\dot{\epsilon}(s)\, ds \tag{5}$$

where the relaxation function is

$$G(t-s) := E_\infty + E\exp\left[-(t-s)/\tau\right] \tag{6}$$

Suppose, now, that we write the strain $\epsilon(t)$ in terms of the creep function $J(t)$ as follows:

$$\epsilon(t) = \int_{-\infty}^{t} J(t-s)\dot{\sigma}(s)\,ds; \quad J(t) = \frac{1}{E_\infty}\left(1 - \frac{E}{E_\infty}\exp\left[\frac{-E_\infty t}{E_0 t}\right]\right) \tag{7}$$

where we apply a step function for the total stress such that,

$$\sigma(t) = \sigma_0 H(t); \quad \dot{\sigma}(t) = \sigma_0 \delta(t) \tag{8}$$

Substitution of the above into Eq. 7_1 gives

$$\epsilon(t) = \int_{-\infty}^{t} J(t-s)\sigma_0\delta(s)\,ds = \sigma_0 J(t) \tag{9}$$

We will compare the effects of a creeping viscoelastic model to that of a poroelastic model, the latter equations of which we will derive in the following section.

1.2.2 Linear Poroelasticity in One Dimension at Small Strain

Terzaghi's 1-D consolidation theory[64] makes the following assumptions:

1. The solid constituent is homogeneous.
2. The porous medium is fully saturated (i.e., there are only two constituents in the porous medium: solid skeleton and pore fluid).
3. The solid constituent and pore fluid constituent are incompressible. Note that the porous solid skeleton "matrix" remains compressible so that deformation may occur.
4. The applied compression is purely vertical in the z direction (i.e., uniaxial strain), and the motion of the pore fluid is purely vertical as well (i.e., unidirectional flow).
5. Darcy's law (sans inertia and body force terms) $v_{z,\mathrm{f}} = -\hat{k}\gamma_\mathrm{f}\frac{dh}{dz}$, is valid, where $v_{z,\mathrm{f}}$ is the pore fluid seepage velocity in the z direction, $\hat{k}$ is the hydraulic conductivity, γ_f is the unit weight of the pore fluid, and h is the pressure head.
6. The results are valid for small strain:

(a) $\hat{k}$ is independent of the void ratio change Δe and is assumed constant during the consolidation process. Note that porosity $n := e/(1+e)$).

(b) m_v, the compressibility factor under uniaxial strain, is assumed constant during the consolidation process (i.e., linear isotropic elasticity will hold).

7. There are no sources or sinks of pore fluid.

From Assumptions 3, 4 and 7, the continuity equation reduces to

$$\frac{dv_{z(\mathrm{f})}}{dz} dxdydz = 0 \tag{10}$$

which we may also write as

$$\frac{dv_{z(\mathrm{f})}}{dz} dxdydz = \frac{dV}{dt} \tag{11}$$

Substitution of Darcy's law into Eq. 10 gives

$$\frac{dv_{z(\mathrm{f})}}{dz} = -\hat{k}\gamma_{\mathrm{f}} \frac{d^2h}{dz^2} \tag{12}$$

where the pressure head is defined as

$$h := \frac{p_{\mathrm{f}}}{\gamma_{\mathrm{f}}} + z \tag{13}$$

and the pore fluid pressure p_{f} may be written as the summation of the fluid unit weight γ_{f} times the position z and an excess pore fluid pressure $p_{\mathrm{f},e}$. Thus, we can rewrite Eq. 12 as

$$\frac{dv_{z(\mathrm{f})}}{dz} = -\hat{k} \frac{d^2 p_{\mathrm{f},e}}{dz^2} \tag{14}$$

Now, assuming a linear isotropic elastic constitutive relation for the volumetric strain for uniaxial strain under vertical stress, we may write

$$\frac{\Delta V}{V} = m_v \Delta \sigma' \tag{15}$$

Rearranging, dividing both sides by Δt and taking the limit as $\Delta t \to 0$ gives us

$$\frac{dV}{dt} = m_v \frac{d\sigma'}{dt} dxdydz \tag{16}$$

Recall the effective stress principle where total stress σ is decomposed into solid skeleton stress σ' and pore fluid pressure p_f (i.e., $\sigma := \sigma' + p_\mathrm{f}$) for compressible solid skeleton and nearly incompressible solid constituent. Here, we assume soil mechanics convention for which the normal components of stress are positive in compression, along with the pore fluid pressure p_f. Decomposing the pore fluid pressure in terms of the hydrostatic and excess pore fluid pressure as $p_\mathrm{f} = \gamma_\mathrm{f} z + p_{\mathrm{f},e}$ and then taking the time derivative of all four terms above provides the useful relation

$$\frac{d\sigma'}{dt} = -\frac{dp_{\mathrm{f},e}}{dt} \tag{17}$$

Substitution of this result back into Eq. 16, equating with Eqs. 11 and 14, and rearranging, gives us the following partial differential equation (PDE) for $p_{\mathrm{f},e}$:

$$\frac{\partial p_{\mathrm{f},e}}{\partial t} = c_v \frac{\partial^2 p_{\mathrm{f},e}}{\partial z^2} \tag{18}$$

where the coefficient of consolidation $c_v = \hat{k}/(m_v \gamma_\mathrm{f})$. We further assume the following "drained" (i.e., atmospheric) boundary conditions:

$$p_{\mathrm{f},e}(0,t) = 0, \quad p_{\mathrm{f},e}(2H,t) = 0 \tag{19}$$

where H is defined as the longest flow path to the drained boundary for a given pore fluid molecule, and an initial pressure along the domain is defined as

$$p_{\mathrm{f},e}(z,0) = p_{\mathrm{f},e,0}(z) \tag{20}$$

Note that a drained boundary condition implies atmospheric pressure, which we assume is referenced to 0 atm. This PDE may be solved using the method of separation of variables where

$$p_{\mathrm{f},e}(z,t) = F(z)\Phi(t) \tag{21}$$

and thus Eq. 18 becomes

$$\frac{1}{F(z)}\frac{\partial^2 F}{\partial z^2} = \frac{1}{c_v \Phi(t)}\frac{\partial \Phi}{\partial t} \tag{22}$$

Since the left- and right-hand sides of Eq. 22 are independent of t and z, respectively, they must both be equal to some constant, which we denote by $-A^2$. Solving for $F(z)$ yields

$$F(z) = c_1 \cos(Az) + c_2 \sin(Az) \tag{23}$$

and likewise solving for $\Phi(t)$ yields

$$\Phi(t) = c_3 \exp\left[-A^2 c_v t\right] \tag{24}$$

Then Eq. 21 may be rewritten as the product of these solutions:

$$p_{\mathrm{f},e} = (c_4 \cos(Az) + c_5 \sin(Az)) \exp\left[-A^2 c_v t\right] \tag{25}$$

where $c_4 = c_1 c_3$ and $c_5 = c_2 c_3$. Using the boundary condition given by Eq. 19_1 gives $c_4 = 0$. Likewise, using the boundary condition given by Eq. 19_2 gives

$$p_{\mathrm{f},e}(2H, t) = 0 = c_5 \sin\left(\frac{n\pi}{2H} z\right) \exp\left[-\left(\frac{n\pi}{2H}\right)^2 c_v t\right] \tag{26}$$

Since c_5 is arbitrary, we may write the solution for the excess pore fluid pressure as a summation over all n as

$$p_{\mathrm{f},e}(z, t) = \sum_{n=1}^{\infty} B_n \sin\left(\frac{n\pi}{2H} z\right) \exp\left[-\left(\frac{n\pi}{2H}\right)^2 c_v t\right] \tag{27}$$

where B_n is a yet to be determined constant. Using our initial condition defined by Eq. 20 allows us to write

$$p_{\mathrm{f},e,0}(z) = \sum_{n=1}^{\infty} B_n \sin\left(\frac{n\pi}{2H} z\right) \tag{28}$$

This is a Fourier sine series, which when multiplied by $\sin(n\pi z/2H)$ allows us to solve for B_n, making use of the orthogonality relation of two sinusoidal waves over

the period $2H$, as

$$B_n = \frac{1}{H} \int_0^{2H} p_{\mathrm{f},e,0}(z) \sin\left(\frac{n\pi}{2H} z\right) dz \tag{29}$$

Substitution of this result back into Eq. 27 gives

$$p_{\mathrm{f},e}(z,t) = \sum_{n=1}^{\infty} \left(\frac{1}{H} \int_0^{2H} p_{\mathrm{f},e,0}(z) \sin\left(\frac{n\pi}{2H} z\right) dz \right) \sin\left(\frac{n\pi}{2H} z\right) \exp\left[-\frac{(n\pi)^2}{4} T\right] \tag{30}$$

where $T = c_v t/H$ is the dimensionless time factor. Consider now the case where the initial excess pore fluid pressure is constant: $p_{\mathrm{f},e,0}(z) = t^\sigma$. Then we may solve for B_n by integrating Eq. 29 directly as

$$B_n = \frac{1}{H} \int_0^{2H} t^\sigma \sin\left(\frac{n\pi}{2H} z\right) dz = \frac{2t^\sigma}{n\pi}(1 - \cos(n\pi)) \tag{31}$$

which gives

$$p_{\mathrm{f},e}(z,t) = \sum_{n=1}^{\infty} \frac{2t^\sigma}{M} \sin\left(\frac{M}{H} z\right) \exp\left[-M^2 T\right] \tag{32}$$

where $M = n\pi/2$.

1.2.3 Comparison of Linear Viscoelasticity and Poroelasticity in One Dimension at Small Strain

We now compare the 1-D uniaxial strain, unidirectional flow poroelastic response to the creep viscoelastic response. Two columns of different heights H are modeled as drawn in Fig. 3. Both columns, each with either of the poroelastic and viscoelastic models, are subject to a Heaviside step function in boundary traction as shown in Fig. 4.

This loading results in a constant initial stress with distance if we ignore gravitational effects. Figure 5 shows that for the shorter column, the relaxation times between the viscoelastic and poroelastic models are identical. For the taller column, the relaxation time for the viscoelastic model is identical to that of the shorter

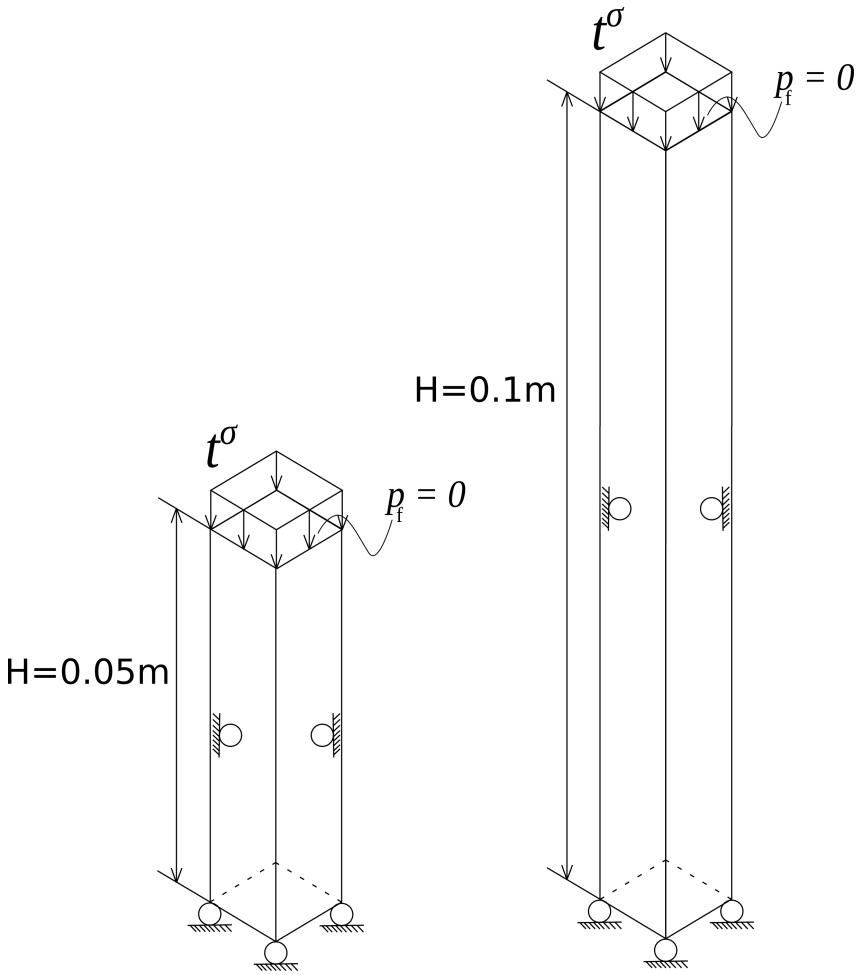

Fig. 3 Schematic of the columns used for a thought experiment. The cross-sectional areas are identical between both, but the second column is double the height of the first.

column. However, the relaxation time is significantly increased for the poroelastic model. This is because the direct consideration of the pore fluid means that the solid skeleton must displace said fluid before reaching steady-state displacement. In the context of lung deformations, this is an important distinction to make because a simple difference in geometry leads to drastically different deformation processes.

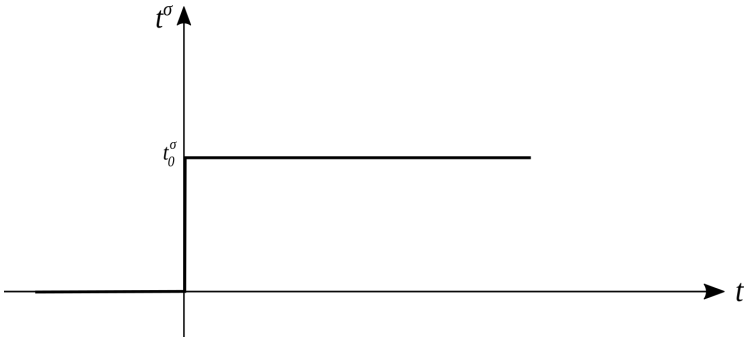

Fig. 4 The applied Heaviside step function applied to the top of the column

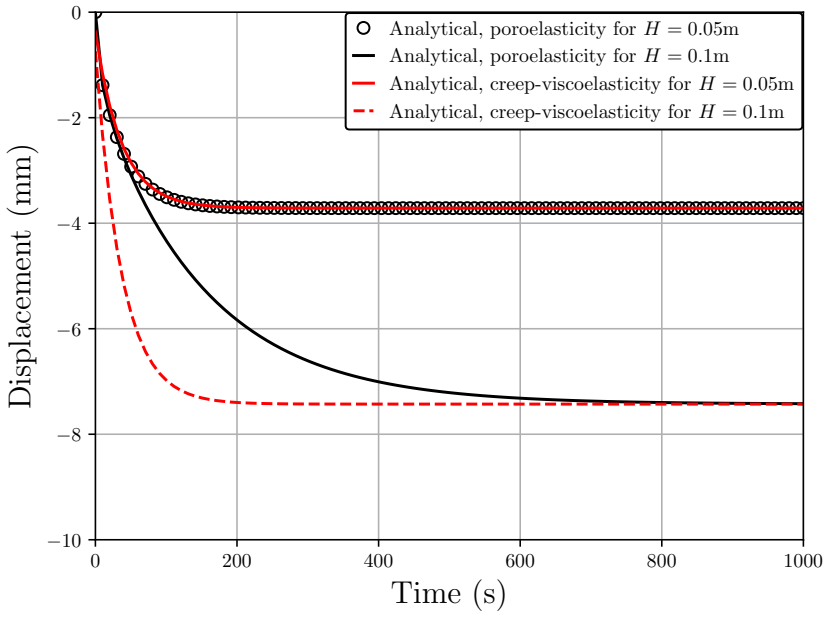

Fig. 5 Comparison for soil sample with initial applied stress $t^\sigma = 100$ kPa

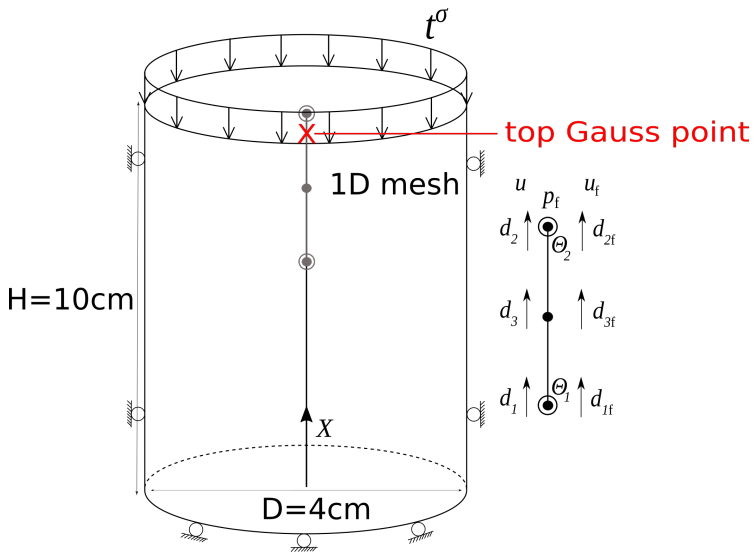

Fig. 6 Schematic for a cylindrical mesh used in the 1-D uniaxial strain simplification, where the Q2-Q2-P1 element[65] is highlighted. Here, d corresponds to the interpolated solid skeleton (s) displacement solution, d_f corresponds to the interpolated pore fluid (f) displacement solution, and θ corresponds to the interpolated pore fluid pressure solution at their respective nodes in the FE model.

1.2.4 Geometric Model

In later analysis,[65,66] we model an excised section of lung parenchyma as either a uniform cylinder or uniform rectangular column. Our choice of geometry is somewhat arbitrary as long as the motion is uniaxial. If we assume uniaxial strain with unidirectional flow (i.e., no permeation of air through the sides of the cylinder), the overall geometry of the lung parenchyma becomes irrelevant because we can reduce it to 1-D. This assumption is appropriate for immediate motions resulting from shock loadings in which the magnitude of transverse motions (i.e., those perpendicular to the direction of the shock front) are small compared to the motions aligned with the direction of the shock front. When making comparisons to other software models, such as those in the LS-DYNA code,[67] we typically assume a rectangular column for ease of meshing in other software frameworks, which has the sole effect of altering the cross-sectional area when compared to the cylindrical column for fixed width or diameter (i.e., cylindrical area of $\pi D^2/4 \approx 12.6$ cm^2, versus rectangular area of $L^2 \approx 1$ cm^2). The cylindrical geometry is shown in Fig. 6, and the rectangular geometry is shown in Fig. 7. These geometries are considered in more depth in subsequent reports on numerical methods and simulations.[65,66]

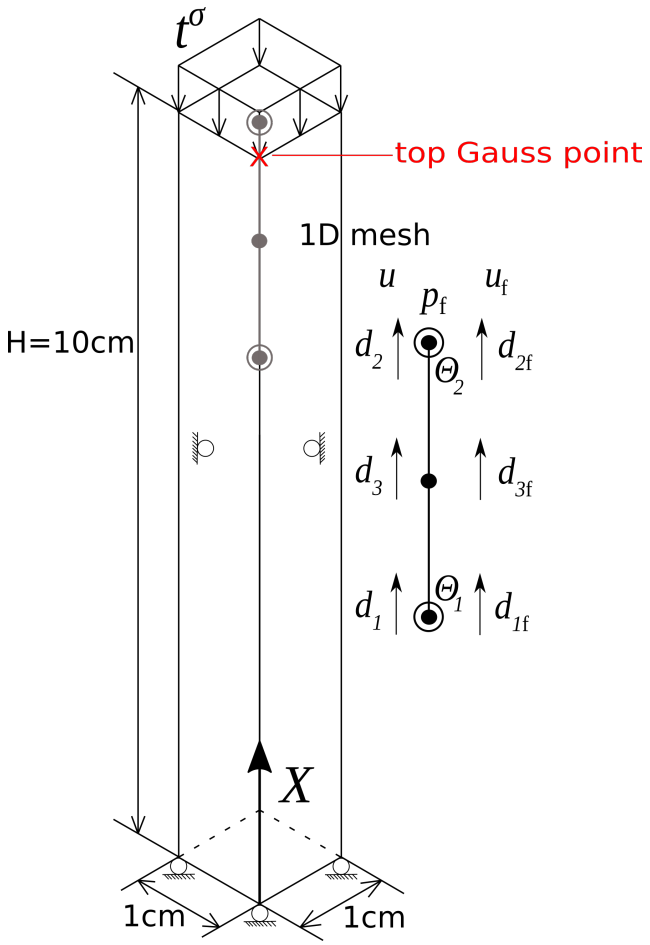

Fig. 7 Schematic for a rectangular mesh used in the 1-D uniaxial strain simplification, where the Q2-Q2-P1 element[65] is highlighted. Here, d corresponds to the interpolated solid skeleton (s) displacement solution, d_{f} corresponds to the interpolated pore fluid (f) displacement solution, and θ corresponds to the interpolated pore fluid pressure solution at their respective nodes in the FE model.

1.3 Organization

The remainder of this report is organized in the following manner. Section 2 introduces concepts for mixture theory and the TPM, and how these theories are applied to porous lung parenchyma. Following this, the physical balance equations are derived for a general constituent α and then derived for the mixture of the two phases: solid (s) and fluid (f). In Section 3, we show how the balance equations allow us to derive our constitutive equations. Conclusions summarizing the theoretical developments and mentioning subsequent applications[65,66,68] follow in Section 4.

The term "elasticity" is used to refer to a quasi-static setting (i.e., inertial terms and stress waves absent) with linear or nonlinear elastic constitutive behavior. The term "elastodynamics" refers to a fully dynamic setting (i.e., inertial terms retained in the momentum balance, leading to stress waves), again with linear or nonlinear elastic behavior.

2. The Theory of Porous Media

An extensive background of TPM is provided by Bowen,[17–19] Coussy,[21] Ehlers[20] and de Boer,[22] and originally in Truesdell and Toupin.[16] We will follow the notation of Holzapfel[69] (for solid mechanics) and de Boer.[22]

2.1 Concept of Volume Fractions

We assume that the porous solid continuum body constitutes a control space $\mathcal{B}$ (current configuration of the solid skeleton) and that only liquids or gases in the pores can leave this control space. Rather than modeling the exact microstructure of the porous solid, we assume that the pores are modeled in a statistical sense such that their specific locations are arbitrary. This concept of volume fraction is illustrated in Fig. 8a. The volume fractions n^α are defined such that they relate the "real" differential volumes dv_α of each constituent, or phase, α to the smeared (i.e., homogenized) total differential volume dv:

$$n^\alpha(\boldsymbol{x}, t) = \frac{dv_\alpha(\boldsymbol{x}, t)}{dv(\boldsymbol{x}, t)} \tag{33}$$

where $\boldsymbol{x}$ is the position vector in the current configuration $\mathcal{B}$ (see Fig.8b), and t is current time. Thus, for any mixture, the constituents α occupying some control

volume dv in the control space $\mathcal{B}$ must satisfy

$$\sum_{\alpha} n^{\alpha}(\boldsymbol{x},t) = 1 \ , \quad \sum_{\alpha} dv_{\alpha}(\boldsymbol{x},t) = dv(\boldsymbol{x},t) \tag{34}$$

We furthermore assume that the constituents are immiscible (following the *principle of phase separation*[20]) such that we can relate the partial mass density ρ^{α}, that is, the mass density of constituent α occupying the total differential volume dv containing multiple constituents, to the real mass density $\rho^{\alpha\mathrm{R}}$, the mass density of constituent α occupying the differential volume dv_{α} containing only constituent α, as follows:

$$\begin{aligned} m_{\alpha}(\boldsymbol{x},t) &= \int_{\mathcal{B}^{\alpha}} \rho^{\alpha\mathrm{R}}(\boldsymbol{x},t) dv_{\alpha}(\boldsymbol{x},t) \\ &= \int_{\mathcal{B}} \rho^{\alpha\mathrm{R}}(\boldsymbol{x},t) n^{\alpha}(\boldsymbol{x},t)\, dv(\boldsymbol{x},t) = \int_{\mathcal{B}} \rho^{\alpha}(\boldsymbol{x},t)\, dv(\boldsymbol{x},t) \end{aligned} \tag{35}$$

where m_{α} is the mass of constituent α in the control space $\mathcal{B}$. Hereafter we assume that variables written in the current configuration $\mathcal{B}$ are dependent on position $\boldsymbol{x}$ at time t so as to simplify the notation. Similarly, variables written in the reference configuration $\mathcal{B}_0$ are dependent on position $\boldsymbol{X}$ at time t.

2.2 Kinematics

The kinematics of a biphasic solid-fluid mixture theory, where $\alpha = \mathrm{s}, \mathrm{f}$, and f is *either* a liquid or a gas, and cannot be decomposed into both as is common in triphasic solid-liquid-gas mixture theory,[22] are shown in Fig. 8b. The vector $\boldsymbol{x}$ is the spatial position vector which is occupied by both constituent material points X_{s} and X_{f} of the mixture such that $\boldsymbol{x} = \boldsymbol{\chi}_{\mathrm{f}}(\boldsymbol{X}_{\mathrm{f}},t) = \boldsymbol{\chi}_{\mathrm{s}}(\boldsymbol{X}_{\mathrm{s}},t)$, where the material point of the solid constituent is mapped from the reference position $\boldsymbol{X}_{\mathrm{s}}$ to the current position $\boldsymbol{x}$ through mapping $\boldsymbol{\chi}_{\mathrm{s}}$. The inverse map is defined as $\boldsymbol{X}_{\alpha} = \boldsymbol{\chi}_{\alpha}^{-1}(\boldsymbol{x},t)$, assuming smoothly differentiable fields. The deformation gradient and its inverse are defined as follows assuming Cartesian coordinates:

$$\begin{aligned} \boldsymbol{F}_{\alpha} &= \frac{\partial \boldsymbol{\chi}_{\alpha}}{\partial \boldsymbol{X}_{\alpha}}, \qquad \boldsymbol{F}_{\alpha}^{-1} = \frac{\partial \boldsymbol{X}_{\alpha}}{\partial \boldsymbol{x}} \\ F_{iI(\alpha)} &= \frac{\partial \chi_{i(\alpha)}}{\partial X_{I(\alpha)}}, \quad F_{Ii(\alpha)}^{-1} = \frac{\partial X_{I(\alpha)}}{\partial x_i} \end{aligned} \tag{36}$$

The differential volumes dV_{f} and dV_{s} in their respective reference configurations

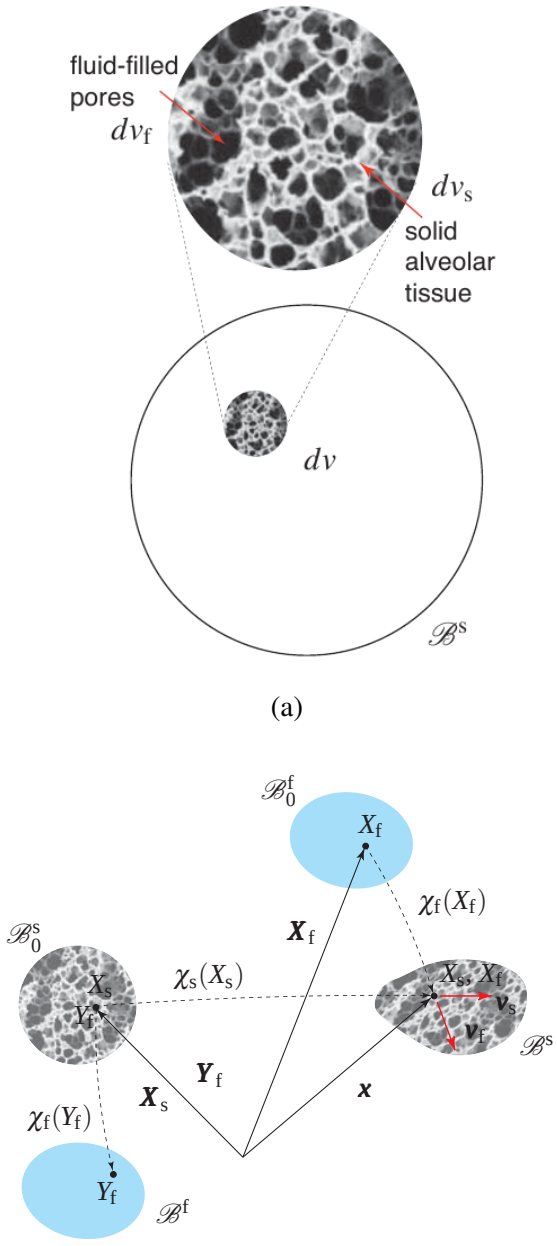

Fig. 8 Concept of volume fraction for biphasic (solid(s)-fluid(f)) mixture theory a), showing solid skeleton composed of alveolar tissue. Note that in the theory of porous media, it is assumed that the control space is that of the solid phase $\mathcal{B} := \mathcal{B}^\mathrm{s}$, also known as "solid skeleton." Kinematics b) of a biphasic (solid-fluid) mixture theory.

$\mathcal{B}_0^\mathrm{f}$ and $\mathcal{B}_0^\mathrm{s}$ both map to the same differential volume dv in the current configuration $\mathcal{B}_t$ through their deformation gradients $\boldsymbol{F}_\mathrm{f}$ and $\boldsymbol{F}_\mathrm{s}$. The Jacobian of deformation for

both constituents is defined as follows:

$$J_{\mathrm{s}} = \det \boldsymbol{F}_{\mathrm{s}} > 0; \quad J_{\mathrm{f}} = \det \boldsymbol{F}_{\mathrm{f}} > 0 \tag{37}$$

$$dv = J_{\mathrm{s}} dV_{\mathrm{s}} = J_{\mathrm{f}} dV_{\mathrm{f}} \tag{38}$$

$$dv_\alpha = n^\alpha \, dv = n^\alpha J_\alpha dV_\alpha \tag{39}$$

$$dV_{\mathrm{f}} \subset \mathcal{B}_0^{\mathrm{f}}, \quad dV_{\mathrm{s}} \subset \mathcal{B}_0^{\mathrm{s}} \tag{40}$$

We will convert all material time derivatives with respect to the solid (s) constituent motion (equivalently, the solid skeleton motion; see note in Fig. 8a for details) such that for constituent α the material time derivative is

$$D_t^\alpha(\square) = \frac{D^\alpha(\square)}{Dt} = \frac{D^{\mathrm{s}}(\square)}{Dt} + \frac{\partial(\square)}{\partial \boldsymbol{x}} \cdot \tilde{\boldsymbol{v}}_\alpha \tag{41}$$

$$\tilde{\boldsymbol{v}}_\alpha = \boldsymbol{v}_\alpha - \boldsymbol{v}_{\mathrm{s}} \tag{42}$$

$$D_t^{\mathrm{s}}(\square) = \frac{D^{\mathrm{s}}(\square)}{Dt} = \frac{\partial(\square)}{\partial t} + \frac{\partial(\square)}{\partial \boldsymbol{x}} \cdot \boldsymbol{v}_{\mathrm{s}} \tag{43}$$

where $\tilde{\boldsymbol{v}}_\alpha$ is the relative velocity vector of the constituent α with respect to the solid (s) constituent motion.

2.3 Balance of Mass

The total mass of a constituent α in the current configuration $\mathcal{B}$ can be written as

$$m_\alpha = \int_{\mathcal{B}} \rho^\alpha dv = \int_{\mathcal{B}_0} \rho^\alpha J_\alpha dV_\alpha \tag{44}$$

After taking the material time derivative of m_α with respect to the motion of α, the balance of mass of constituent α can be written as

$$D_t^\alpha m_\alpha = \int_{\mathcal{B}} \left(D_t^\alpha \rho^\alpha + \rho^\alpha \operatorname{div} \boldsymbol{v}_\alpha \right) dv = \int_{\mathcal{B}} \hat{\gamma}^\alpha \, dv \tag{45}$$

where $\hat{\gamma}^\alpha$ is the mass supply of constituent α per unit total current volume. The local form of Eq. 45 is, upon dividing by $\rho^{\alpha \mathrm{R}}$,

$$D_t^\alpha n^\alpha + \frac{n^\alpha}{\rho^{\alpha \mathrm{R}}} D_t^\alpha \rho^{\alpha \mathrm{R}} + n^\alpha \operatorname{div} \boldsymbol{v}_\alpha = \frac{\hat{\gamma}^\alpha}{\rho^{\alpha \mathrm{R}}} \tag{46}$$

We assume that there is no supply of solid mass to the solid (s) constituent such that $\hat{\gamma}^{\mathrm{s}} \to 0$, and that the solid (s) constituent of the soft porous material (i.e., the solid skeleton wall material) is both *thermally* and *mechanically* incompressible: $\rho^{\mathrm{sR}} :=$ constant.

Following this, we may proceed with a constitutive assumption for the internal energy function of the fluid phase: it produces a pressure that depends only on its real mass density: $p_{\mathrm{f}} = p_{\mathrm{f}}(\rho^{\mathrm{fR}})$. Denoting the isentropic bulk modulus[61,70] of the pore fluid by K_{f}^{η},

$$K_{\mathrm{f}}^{\eta} := \rho^{\mathrm{fR}} \frac{\partial p_{\mathrm{f}}}{\partial \rho^{\mathrm{fR}}}\Big|_{\eta^{\mathrm{f}}} \tag{47}$$

Suppose then that pore fluid pressure is defined as $p_{\mathrm{f}}(v^{\mathrm{f}})$ where v^{f} is the specific volume of the pore fluid. It follows that

$$D_t^{\mathrm{f}} p_{\mathrm{f}} = \frac{\partial p_{\mathrm{f}}}{\partial v^{\mathrm{f}}}\Big|_{\eta^{\mathrm{f}}} D_t^{\mathrm{f}} v^{\mathrm{f}} \tag{48}$$

Then, using the definition given in Eq. 47,

$$D_t^{\mathrm{f}} p_{\mathrm{f}} = \frac{K_{\mathrm{f}}^{\eta}}{\rho^{\mathrm{fR}}} D_t^{\mathrm{f}} \rho^{\mathrm{fR}} \tag{49}$$

Next, as we express the balance of mass for both constituents (i.e., the solid and fluid) individually, the incompressibility assumption $D_t^{\alpha}\rho^{\alpha\mathrm{R}} \to 0$ is used for the solid phase in Eq. 46 for $\alpha = \mathrm{s}$ and Eq. 49 is used in Eq. 46 for $\alpha = \mathrm{f}$. Adding these two equations together, then using the relationship between volume fractions $n^{\mathrm{f}} = 1 - n^{\mathrm{s}}$, the combined balance of mass of the mixture becomes

$$\frac{n^{\mathrm{f}}}{K_{\mathrm{f}}^{\eta}} D_t^{\mathrm{s}} p_{\mathrm{f}} + \operatorname{div} \boldsymbol{v}_{\mathrm{s}} + \frac{1}{K_{\mathrm{f}}^{\eta}} \operatorname{grad}(p_{\mathrm{f}}) \cdot (n^{\mathrm{f}} \tilde{\boldsymbol{v}}_{\mathrm{f}}) + \operatorname{div}(n^{\mathrm{f}} \tilde{\boldsymbol{v}}_{\mathrm{f}}) = \frac{\hat{\gamma}^{\mathrm{f}}}{\rho^{\mathrm{fR}}} \tag{50}$$

We can map Eq. 50 back to the reference configuration of the solid skeleton $\mathcal{B}_0 = \mathcal{B}_0^{\mathrm{s}}$ as

$$\begin{aligned} &\frac{J_{\mathrm{s}} n^{\mathrm{f}}}{K_{\mathrm{f}}^{\eta}} D_t^{\mathrm{s}} p_{\mathrm{f}} + D_t^{\mathrm{s}} J_{\mathrm{s}} \\ &\qquad + \frac{J_{\mathrm{s}}}{K_{\mathrm{f}}^{\eta}} \operatorname{GRAD}_{\mathrm{s}}(p_{\mathrm{f}}) \cdot \boldsymbol{F}_{\mathrm{s}}^{-1} \cdot (n^{\mathrm{f}} \tilde{\boldsymbol{v}}_{\mathrm{f}}) + J_{\mathrm{s}} \operatorname{GRAD}_{\mathrm{s}}(n^{\mathrm{f}} \tilde{\boldsymbol{v}}_{\mathrm{f}}) : \boldsymbol{F}_{\mathrm{s}}^{-T} = \frac{J_{\mathrm{s}} \hat{\gamma}^{\mathrm{f}}}{\rho^{\mathrm{fR}}} \end{aligned} \tag{51}$$

where subscript or superscript s implies with respect to the motion of the solid skeleton.

2.4 Balance of Linear Momentum

The balance of linear momentum for constituent α is written as

$$D_t^\alpha \left(\int_{\mathcal{B}} \rho^\alpha \boldsymbol{v}_\alpha \, dv \right) = \int_{\mathcal{B}} \rho^\alpha \boldsymbol{b}^\alpha \, dv + \int_{\Gamma} \boldsymbol{t}^\alpha \, da + \int_{\mathcal{B}} \boldsymbol{h}^\alpha \, dv \tag{52}$$

After carrying through the material time derivative and applying the balance of mass given by Eq. 45, applying the divergence theorem to the traction term $\boldsymbol{t}^\alpha$, and localizing the integral, we may write

$$\operatorname{div} \boldsymbol{\sigma}^\alpha + \rho^\alpha \boldsymbol{b}^\alpha + \boldsymbol{h}^\alpha = \rho^\alpha \boldsymbol{a}_\alpha + \hat{\gamma}^\alpha \boldsymbol{v}_\alpha \tag{53}$$

where $\boldsymbol{\sigma}^\alpha$ is the partial Cauchy stress, such that the total Cauchy stress $\boldsymbol{\sigma} = \boldsymbol{\sigma}^{\mathrm{s}} + \boldsymbol{\sigma}^{\mathrm{f}}$, ρ^α is the partial mass density (total mass density $\rho = \rho^{\mathrm{s}} + \rho^{\mathrm{f}}$), $\boldsymbol{b}^\alpha$ is the body force per unit mass on constituent α (e.g., acceleration due to gravity such that $\boldsymbol{b}^\alpha = \boldsymbol{g}$), $\boldsymbol{h}^\alpha$ is the interaction body force from all other constituents on constituent α, $\boldsymbol{a}_\alpha$ is the acceleration vector, and $\hat{\gamma}^\alpha \boldsymbol{v}_\alpha$ is the mass supply momentum, which we typically assume is negligible. Usually, the interaction body forces between constituents are due to drag and will sum to zero because they are equal and opposite. Thus, these forces do not affect the mixture as a whole such that $\boldsymbol{h}^{\mathrm{s}} + \boldsymbol{h}^{\mathrm{f}} = \boldsymbol{0}$. Via the balance of angular momentum, it can be shown that the partial Cauchy stresses for each constituent α are symmetric: $\boldsymbol{\sigma}^\alpha = (\boldsymbol{\sigma}^\alpha)^T$.

Equation 53 can be mapped back to the reference configuration of the solid skeleton for constituent α as

$$\mathrm{DIV}_{\mathrm{s}} \boldsymbol{P}_{\mathrm{s}}^\alpha + \rho_{0(\mathrm{s})}^\alpha \boldsymbol{b}^\alpha + J_{\mathrm{s}} \boldsymbol{h}^\alpha = \rho_{0(\mathrm{s})}^\alpha \boldsymbol{a}_\alpha + \hat{\gamma}_{0(\mathrm{s})}^\alpha \boldsymbol{v}_\alpha \tag{54}$$

where again, subscript s or (s) implies with respect to solid skeleton reference configuration, such that $\rho_{0(\mathrm{s})}^\alpha = J_{\mathrm{s}} \rho^\alpha$. From Eq. 54 we can derive the balance of linear momentum equation for the biphasic mixture in the reference configuration $\mathcal{B}_0^{\mathrm{s}}$ using the following equations and assumptions:

1. Mixed constituent temperatures: $\theta^{\mathrm{f}} = \theta^{\mathrm{s}} = \theta$

2. Total Cauchy stress, and first Piola stress with respect to $\mathcal{B}_0^{\mathrm{s}}$:

$$\boldsymbol{\sigma} = \boldsymbol{\sigma}^{\mathrm{s}} + \boldsymbol{\sigma}^{\mathrm{f}} \ , \ \boldsymbol{P}_{\mathrm{s}} = \boldsymbol{P}_{\mathrm{s}}^{\mathrm{s}} + \boldsymbol{P}_{\mathrm{s}}^{\mathrm{f}} \tag{55}$$

3. Decomposition of the solid partial Cauchy stress into an extra stress, hereafter referred to as the solid skeleton effective stress, and pore fluid pressure (justified in Section 3, see also Ehlers[20]):

$$\boldsymbol{\sigma}^{\mathrm{s}} = \boldsymbol{\sigma}_E^{\mathrm{s}} - p_{\mathrm{f}} n^{\mathrm{s}} \mathbf{1} \tag{56}$$

4. Assume all mass supplies are negligible: $\hat{\gamma}^{\alpha} = 0$

5. Assume body forces per unit mass are only due to gravity: $\boldsymbol{b}^{\alpha} = \boldsymbol{g}$, where $\boldsymbol{g}$ is the acceleration vector of gravity.

We may then write the balance of linear momentum equation for the biphasic mixture in the reference configuration $\mathcal{B}_0^{\mathrm{s}}$ as

$$\mathrm{DIV}_{\mathrm{s}} \boldsymbol{P}_{\mathrm{s}} + \rho_{0(\mathrm{s})} \boldsymbol{g} = \rho_{0(\mathrm{s})}^{\mathrm{s}} \boldsymbol{a}_{\mathrm{s}} + \rho_{0(\mathrm{s})}^{\mathrm{f}} \boldsymbol{a}_{\mathrm{f}} \tag{57}$$

$$\boldsymbol{P}_{\mathrm{s}} = \boldsymbol{P}_E^{\mathrm{s}} + \boldsymbol{P}_E^{\mathrm{f}} - J_{\mathrm{s}} p_{\mathrm{f}} \boldsymbol{F}_{\mathrm{s}}^{-T} \tag{58}$$

where for the two-field formulation, we will further assume that $\boldsymbol{a}_{\mathrm{f}} \approx \boldsymbol{a}_{\mathrm{s}} = \boldsymbol{a}$, which should be valid only for slower dynamic loadings. With that assumption in mind, the pore fluid viscous stress tensor $\boldsymbol{P}_E^{\mathrm{f}}$ drops from Eq. 58 because the constitutive law that defines it in Section 3 includes spatial dependence on pore fluid velocity, which cannot be determined without a third governing equation for the pore fluid velocity. Note that under the assumption of a nearly inviscid pore fluid ($\boldsymbol{\sigma}_E^{\mathrm{f}} \to 0$), Eq. 58 may be rewritten as

$$\boldsymbol{P}_{\mathrm{s}} = \boldsymbol{P}_E^{\mathrm{s}} - J_{\mathrm{s}} p_{\mathrm{f}} \boldsymbol{F}_{\mathrm{s}}^{-T} \tag{59}$$

2.5 Balance of Linear Momentum of Pore Fluid

Equation 57 allows us to solve for the displacement of the solid skeleton (i.e., the connective tissue network of the soft porous material), but not for the displacement or velocity of the pore fluid (f) phase. Thus, we require an additional governing equation.

As motivated by satisfying the second law of thermodynamics in Clausius-Duhem form (see Coussy[21] or de Boer[22]), upon substitution of the balance of linear momentum of the pore fluid and neglecting the pore fluid extra stress (i.e., the viscous component of total pore fluid stress), a generalized Darcy's law may be formulated, which relates the smeared relative velocity of the fluid to the Cauchy pore fluid pressure gradient, fluid acceleration, and body force, such that

$$n^{\mathrm{f}}\tilde{\boldsymbol{v}}_{\mathrm{f}} = -\hat{k}\left[\mathrm{grad}p_{\mathrm{f}} + \rho^{\mathrm{fR}}(\boldsymbol{a}_{\mathrm{f}} - \boldsymbol{b}^{\mathrm{f}})\right] \tag{60}$$

where $\hat{k}$ is the hydraulic conductivity, a proportionality parameter in the Clausius-Duhem inequality, that may be a function of fluid volume fraction n^{f} (i.e., porosity), and where it has been assumed that the solid skeleton's permeability is isotropic. Rewriting Eq. 60 after multiplying through by n^{f}, and assuming $\boldsymbol{b}^{\mathrm{f}} = \boldsymbol{b}^{\mathrm{s}} = \boldsymbol{b} = \boldsymbol{g}$, we have

$$\rho^{\mathrm{f}}\boldsymbol{a}_{\mathrm{f}} + n^{\mathrm{f}}\mathrm{grad}p_{\mathrm{f}} + \frac{(n^{\mathrm{f}})^2}{\hat{k}}(\boldsymbol{v}_{\mathrm{f}} - \boldsymbol{v}_{\mathrm{s}}) - \rho^{\mathrm{f}}\boldsymbol{g} = \boldsymbol{0} \tag{61}$$

We can map this to the reference configuration $\mathcal{B}_0^{\mathrm{s}}$,

$$\rho^{\mathrm{f}}_{0(\mathrm{s})}\boldsymbol{a}_{\mathrm{f}} + J_{\mathrm{s}}n^{\mathrm{f}}\,\mathrm{GRAD}_{\mathrm{s}}\,p_{\mathrm{f}}\cdot\boldsymbol{F}_{\mathrm{s}}^{-1} + \frac{J_{\mathrm{s}}(n^{\mathrm{f}})^2}{\hat{k}}(\boldsymbol{v}_{\mathrm{f}} - \boldsymbol{v}_{\mathrm{s}}) - \rho^{\mathrm{f}}_{0(\mathrm{s})}\boldsymbol{g} = \boldsymbol{0} \tag{62}$$

Now we have three coupled governing equations that describe the kinematics of the biphasic mixture: Eqs. 51, 57, and 62. We can use these equations to solve for three unknown "fields" (i.e., three solution variables): Cauchy pore fluid pressure p_{f}, solid skeleton displacement $\boldsymbol{u}$ (dropping subscript s), and pore fluid displacement $\boldsymbol{u}_{\mathrm{f}}$, respectively. This is commonly known as the ($\boldsymbol{u}$-$\boldsymbol{u}_{\mathrm{f}}$-$p_{\mathrm{f}}$) formulation. In the ($\boldsymbol{u}$-$p_{\mathrm{f}}$) formulation, we assume that the acceleration of the pore fluid (f) constituent is approximately equal to the acceleration of the solid skeleton via $\boldsymbol{a}_{\mathrm{f}} \approx \boldsymbol{a}_{\mathrm{s}} = \boldsymbol{a}$. Thus, we do not need to solve Eq. 62. We employ variational forms of these equations in the total Lagrangian FE formulation in a follow-up report.[65]

To describe the evolution of phase entropies and temperatures, additional governing equations are required, irrespective of whether or not thermo-mechanical coupling and/or the mixed-temperature constituents are assumed. The governing equations that describe the thermodynamics will end up being the balance of energy of each phase, or the mixture, whichever is more appropriate. Note that in the context of the

current application (i.e., high strain-rate loading of lung parenchyma), a mixture energy balance may not be appropriate given the disparity in thermodynamic material properties between the constituents. Regardless, constitutive relations must be determined prior to numerical implementation of any balance equations. The process for determining constitutive equations essentially begins in the next three subsections, and it concludes with more details in Section 3.

2.6 Balance of Energy

The first law of thermodynamics provides the balance of energy for the mixture as a whole, and can be written in the current configuration $\mathcal{B}$ for phase α as

$$D_t^\alpha \left[K^\alpha(t) + E^\alpha(t)\right] = P_{\text{ext}}^\alpha(t) + Q^\alpha(t) + \bar{E}^\alpha(t) \tag{63}$$

where the kinetic energy is defined as

$$K^\alpha(t) = \int_{\mathcal{B}} \frac{1}{2}\rho^\alpha \boldsymbol{v}_\alpha \cdot \boldsymbol{v}_\alpha dv \tag{64}$$

The internal energy is defined as

$$P_{\text{int}}^\alpha(t) = D_t^\alpha E^\alpha(t) = D_t^\alpha \int_{\mathcal{B}} \rho^\alpha e^\alpha(\boldsymbol{x}, t) dv \tag{65}$$

where the e^α is the internal energy per unit mass, sometimes referred to as ε^α in other works on mixture theory and TPM.[17,22] The external work on phase α is defined as

$$P_{\text{ext}}^\alpha(t) = \int_\Gamma \boldsymbol{t}^\alpha \cdot \boldsymbol{v}_\alpha da + \int_{\mathcal{B}} \rho^\alpha \boldsymbol{b}^\alpha \cdot \boldsymbol{v}_\alpha dv \tag{66}$$

where $\boldsymbol{t}^\alpha = \boldsymbol{n} \cdot \boldsymbol{\sigma}^\alpha$ and $\Gamma := \partial\mathcal{B}$. The rate of thermal work (i.e., the thermal power) acting on an individual constituent is

$$Q^\alpha(t) = -\int_\Gamma \boldsymbol{q}^\alpha \cdot \boldsymbol{n} da + \int_{\mathcal{B}} \rho^\alpha r^\alpha dv \tag{67}$$

where for phase α, $\boldsymbol{q}^\alpha$ is the heat flux vector, and r^α is the heat input rate per unit

mass. Lastly, the power supply to phase α by other phases is defined as

$$\bar{E}^{\alpha}(t) = \int\limits_{\mathcal{B}} \hat{e}^{\alpha} dv = \int\limits_{\mathcal{B}} \Big(\hat{\varepsilon}^{\alpha} + \boldsymbol{h}^{\alpha} \cdot \boldsymbol{v}_{\alpha} + \hat{\gamma}^{\alpha} \Big[e^{\alpha} + \frac{1}{2} \boldsymbol{v}_{\alpha} \cdot \boldsymbol{v}_{\alpha} \Big] \Big) dv \tag{68}$$

where $\hat{\varepsilon}^{\alpha}$ arises from local interaction[17] for energy supply to phase α from other phases and $\hat{e}^{\alpha}$ is the total power density per unit volume supplied to phase α by other phases.

Combining the above energy terms, Eqs. 64–68, the first law of thermodynamics may be written as follows:

$$\begin{aligned} D_t^{\alpha} \int\limits_{\mathcal{B}} \left(\frac{1}{2} \rho^{\alpha} \boldsymbol{v}_{\alpha} \cdot \boldsymbol{v}_{\alpha} + \rho^{\alpha} e^{\alpha} \right) dv = & \int\limits_{\Gamma} \boldsymbol{t}^{\alpha} \cdot \boldsymbol{v}_{\alpha} da + \int\limits_{\mathcal{B}} \rho^{\alpha} \boldsymbol{b}^{\alpha} \cdot \boldsymbol{v}_{\alpha} dv \\ & - \int\limits_{\Gamma} \boldsymbol{q}^{\alpha} \cdot \boldsymbol{n} da + \int\limits_{\mathcal{B}} (\rho^{\alpha} r^{\alpha} + \hat{e}^{\alpha}) dv \end{aligned} \tag{69}$$

Start by applying the material time derivative to switch to reference configuration $\mathcal{B}_0^{\alpha}$:

$$D_t^{\alpha} \int\limits_{\mathcal{B}} \Big(\frac{1}{2} \rho^{\alpha} \boldsymbol{v}_{\alpha} \cdot \boldsymbol{v}_{\alpha} + \rho^{\alpha} e^{\alpha} \Big) dv = D_t^{\alpha} \int\limits_{\mathcal{B}_0^{\alpha}} \Big(\frac{1}{2} \rho^{\alpha} \boldsymbol{v}_{\alpha} \cdot \boldsymbol{v}_{\alpha} + \rho^{\alpha} e^{\alpha} \Big) J_{\alpha} dV_{\alpha} \tag{70}$$

Carry out material time derivative in reference configuration $\mathcal{B}_0^{\alpha}$:

$$\begin{aligned} D_t^{\alpha} \int\limits_{\mathcal{B}_0^{\alpha}} \Big(\frac{1}{2} \rho^{\alpha} \boldsymbol{v}_{\alpha} \cdot \boldsymbol{v}_{\alpha} + \rho^{\alpha} e^{\alpha} \Big) J_{\alpha} dV_{\alpha} = & \int\limits_{\mathcal{B}_0^{\alpha}} \Big(\Big[D_t^{\alpha} \boldsymbol{v}_{\alpha} \cdot \boldsymbol{v}_{\alpha} + D_t^{\alpha} e^{\alpha} \Big] (\rho^{\alpha} J_{\alpha}) \\ & + \Big[\frac{1}{2} \boldsymbol{v}_{\alpha} \cdot \boldsymbol{v}_{\alpha} + e^{\alpha} \Big] \Big[D_t^{\alpha} \rho^{\alpha} J_{\alpha} + \rho^{\alpha} D_t^{\alpha} J_{\alpha} \Big] \Big) dV_{\alpha} \end{aligned} \tag{71}$$

The first term in first set of brackets [ ] on the right-hand side (rhs) of Eq. 71 is acceleration of phase α:

$$D_t^{\alpha} \boldsymbol{v}_{\alpha} := \boldsymbol{a}_{\alpha} \tag{72}$$

Substitution of Eq. 72 gives

$$\Big[D_t^{\alpha} \boldsymbol{v}_{\alpha} \cdot \boldsymbol{v}_{\alpha} + D_t^{\alpha} e^{\alpha} \Big] (\rho^{\alpha} J_{\alpha}) = \Big[\boldsymbol{a}_{\alpha} \cdot \boldsymbol{v}_{\alpha} + D_t^{\alpha} e^{\alpha} \Big] (\rho^{\alpha} J_{\alpha}) \tag{73}$$

The first term in the third set of brackets [ ] on rhs of Eq. 71 is evaluated from balance of mass:

$$D_t^\alpha \rho^\alpha = \hat{\gamma}^\alpha - \rho^\alpha \operatorname{div} \boldsymbol{v}_\alpha \tag{74}$$

The second term in third set of brackets [ ] on rhs of Eq. 71 is evaluated from the continuity equation:

$$D_t^\alpha J_\alpha = J_\alpha \operatorname{div} \boldsymbol{v}_\alpha \tag{75}$$

Substitution and simplification of these two gives

$$\Big[\frac{1}{2}\boldsymbol{v}_\alpha \cdot \boldsymbol{v}_\alpha + e^\alpha\Big]\Big[D_t^\alpha \rho^\alpha J_\alpha + \rho^\alpha D_t^\alpha J_\alpha\Big] = \hat{\gamma}^\alpha \Big[\frac{1}{2}\boldsymbol{v}_\alpha \cdot \boldsymbol{v}_\alpha + e^\alpha\Big] J_\alpha \tag{76}$$

Rewriting the material time derivative of total internal energy in current configuration such that $J_\alpha dV_\alpha \to dv$:

$$\begin{aligned} D_t^\alpha \int_{\mathcal{B}} &\left(\frac{1}{2}\rho^\alpha \boldsymbol{v}_\alpha \cdot \boldsymbol{v}_\alpha + \rho^\alpha e^\alpha\right) dv \\ &= \int_{\mathcal{B}} \Big(\rho^\alpha \boldsymbol{a}_\alpha \cdot \boldsymbol{v}_\alpha + \rho^\alpha D_t^\alpha e^\alpha + \hat{\gamma}^\alpha \Big[e^\alpha + \frac{1}{2}\boldsymbol{v}_\alpha \cdot \boldsymbol{v}_\alpha\Big]\Big) dv \end{aligned} \tag{77}$$

Next, apply divergence theorem to the boundary terms (external work via traction, rate of thermal work via heat flux):

$$\int_\Gamma \boldsymbol{t}^\alpha \cdot \boldsymbol{v}_\alpha da = \int_{\mathcal{B}} \operatorname{div}(\boldsymbol{\sigma}^\alpha \cdot \boldsymbol{v}_\alpha) dv \tag{78}$$

$$\int_\Gamma \boldsymbol{q}^\alpha \cdot \boldsymbol{n} da = \int_{\mathcal{B}} \operatorname{div} \boldsymbol{q}^\alpha dv \tag{79}$$

Expand divergence on Cauchy stress and velocity:

$$\operatorname{div}(\boldsymbol{\sigma}^\alpha \cdot \boldsymbol{v}_\alpha) = \operatorname{div}(\boldsymbol{\sigma}^\alpha) \cdot \boldsymbol{v}_\alpha + \boldsymbol{\sigma} : \boldsymbol{l}_\alpha \tag{80}$$

where $\boldsymbol{l}_\alpha$ is the velocity gradient. Next, apply localization theorem such that the

energy balance for phase α is written as

$$\rho^\alpha \boldsymbol{a}_\alpha \cdot \boldsymbol{v}_\alpha + \rho^\alpha D_t^\alpha e^\alpha + \hat{\gamma}^\alpha \Big(e^\alpha + \frac{1}{2} \boldsymbol{v}_\alpha \cdot \boldsymbol{v}_\alpha \Big) = \operatorname{div}(\boldsymbol{\sigma}^\alpha) \cdot \boldsymbol{v}_\alpha + \boldsymbol{\sigma} : \boldsymbol{l}_\alpha + \rho^\alpha \boldsymbol{b}^\alpha \cdot \boldsymbol{v}_\alpha - \operatorname{div} \boldsymbol{q}^\alpha + \rho^\alpha r^\alpha + \hat{e}^\alpha \tag{81}$$

Third term on rhs of Eq. 81 can be rewritten by substituting balance of momentum:

$$\rho^\alpha \boldsymbol{b}^\alpha = \rho^\alpha \boldsymbol{a}_\alpha + \hat{\gamma}^\alpha \boldsymbol{v}_\alpha - \operatorname{div} \boldsymbol{\sigma}^\alpha - \boldsymbol{h}^\alpha \tag{82}$$

Substitute into Eq. 81:

$$\begin{aligned} \rho^\alpha \boldsymbol{a}_\alpha \cdot \boldsymbol{v}_\alpha + \rho^\alpha D_t^\alpha e^\alpha + \hat{\gamma}^\alpha \Big(e^\alpha + \frac{1}{2} \boldsymbol{v}_\alpha \cdot \boldsymbol{v}_\alpha \Big) &= \operatorname{div}(\boldsymbol{\sigma})^\alpha \cdot \boldsymbol{v}_\alpha + \boldsymbol{\sigma} : \boldsymbol{l}_\alpha \\ + (\rho^\alpha \boldsymbol{a}_\alpha + \hat{\gamma}^\alpha \boldsymbol{v}_\alpha - \operatorname{div} \boldsymbol{\sigma}^\alpha - \boldsymbol{h}^\alpha) \cdot \boldsymbol{v}_\alpha - \operatorname{div} \boldsymbol{q}^\alpha + \rho^\alpha r^\alpha + \hat{e}^\alpha \end{aligned} \tag{83}$$

The acceleration terms and divergence on partial Cauchy stress terms cancel, leaving

$$\rho^\alpha D_t^\alpha e^\alpha = \boldsymbol{\sigma} : \boldsymbol{l}_\alpha - \operatorname{div} \boldsymbol{q}^\alpha + \rho^\alpha r^\alpha + \hat{e}^\alpha + \hat{\gamma}^\alpha \Big(\frac{1}{2} \boldsymbol{v}_\alpha \cdot \boldsymbol{v}_\alpha - e^\alpha \Big) - \boldsymbol{h}^\alpha \cdot \boldsymbol{v}_\alpha \tag{84}$$

Note that this is equivalent to the derivation provided by Bowen[17] if one substitutes the definition of the total power density supply given by Eq. 68 such that

$$\rho^\alpha D_t^\alpha e^\alpha = \boldsymbol{\sigma}^\alpha : \boldsymbol{l}_\alpha - \operatorname{div} \boldsymbol{q}^\alpha + \rho^\alpha r^\alpha + \hat{\varepsilon}^\alpha \tag{85}$$

2.7 Entropy Imbalance

Deriving an entropy imbalance for the mixture as a whole is preferred to deriving one for individual constituents given that the latter can lead to incomplete constitutive relations.[22] We write

$$\sum_\alpha \Gamma^\alpha(t) \geq 0 \tag{86}$$

wherein

$$\Gamma^\alpha(t) = D_t^\alpha H^\alpha(t) - \tilde{Q}^\alpha(t) \tag{87}$$

Thus, the imbalance of entropy can be written in the current configuration $\mathcal{B}$ as

$$\sum_{\alpha} D_t^{\alpha} H^{\alpha}(t) \geq \sum_{\alpha} \tilde{Q}^{\alpha}(t) \tag{88}$$

where the total internal entropy of phase α is

$$H^{\alpha}(t) = \int_{\mathcal{B}} \rho^{\alpha} \eta^{\alpha} dv \tag{89}$$

and the rate of total entropy input for phase α is

$$\tilde{Q}^{\alpha}(t) = \int_{\mathcal{B}} \frac{1}{\theta^{\alpha}} \rho^{\alpha} r^{\alpha} dv - \int_{\Gamma} \frac{1}{\theta^{\alpha}} \boldsymbol{q}^{\alpha} \cdot \boldsymbol{n} da \tag{90}$$

Start by applying the material time derivative to switch to reference configuration $\mathcal{B}_0^{\alpha}$:

$$D_t^{\alpha} \int_{\mathcal{B}} \rho^{\alpha} \eta^{\alpha} dv = D_t^{\alpha} \int_{\mathcal{B}_0^{\alpha}} \rho^{\alpha} \eta^{\alpha} J_{\alpha} dV_{\alpha} \tag{91}$$

Carry out material time derivative in reference configuration $\mathcal{B}_0^{\alpha}$:

$$D_t^{\alpha} \int_{\mathcal{B}_0^{\alpha}} \rho^{\alpha} \eta^{\alpha} J_{\alpha} dV_{\alpha} = \int_{\mathcal{B}_0^{\alpha}} \Big((\eta^{\alpha} J_{\alpha}) D_t^{\alpha} \rho^{\alpha} + (\rho^{\alpha} J_{\alpha}) D_t^{\alpha} \eta^{\alpha} + (\rho^{\alpha} \eta^{\alpha}) D_t^{\alpha} J_{\alpha} \Big) dV_{\alpha} \tag{92}$$

The first and last terms are simplified using mass balance and continuity equation, per Eqs. 74 and 75, respectively, such that

$$D_t^{\alpha} \int_{\mathcal{B}_0^{\alpha}} \rho^{\alpha} \eta^{\alpha} J_{\alpha} dV_{\alpha} = \int_{\mathcal{B}_0^{\alpha}} \Big(\eta^{\alpha} J_{\alpha} \hat{\gamma}^{\alpha} + (\rho^{\alpha} J_{\alpha}) D_t^{\alpha} \eta^{\alpha} \Big) dV_{\alpha} \tag{93}$$

Rewrite the material time derivative of total internal entropy in current configuration such that $J_{\alpha} dV_{\alpha} \to dv$:

$$D_t^{\alpha} \int_{\mathcal{B}} \rho^{\alpha} \eta^{\alpha} dv = \int_{\mathcal{B}} \Big(\eta^{\alpha} \hat{\gamma}^{\alpha} + \rho^{\alpha} D_t^{\alpha} \eta^{\alpha} \Big) dv \tag{94}$$

Apply divergence theorem to the heat flux term in rate of entropy input, Eq. 90:

$$\int_{\Gamma} \frac{1}{\theta^\alpha} \boldsymbol{q}^\alpha \cdot \boldsymbol{n} da = \int_{\mathcal{B}} \operatorname{div}\Big(\frac{1}{\theta^\alpha}\boldsymbol{q}^\alpha\Big) dv \tag{95}$$

Finally, apply localization theorem such that entropy imbalance is written as

$$\sum_\alpha \Big(\hat{\gamma}^\alpha \eta^\alpha + \rho^\alpha D_t^\alpha \eta^\alpha - \frac{1}{\theta^\alpha}\rho^\alpha r^\alpha + \operatorname{div}\Big[\frac{1}{\theta^\alpha}\boldsymbol{q}^\alpha\Big]\Big) \geq 0 \tag{96}$$

2.8 Dissipation Inequality

In order to produce constitutive relations that adhere to the thermodynamic principles laid out by Truesdell and Toupin[16] and Coleman and Noll,[71] the second and first laws will be combined to form the dissipation inequality, that is, the Clausius-Duhem inequality. Introduce the Helmholtz free energy potential for each phase as

$$\psi^\alpha = e^\alpha - \theta^\alpha \eta^\alpha \tag{97}$$

and substitute it into the first law, Eq. 84, such that

$$\begin{aligned} &\rho^\alpha D_t^\alpha \big(\psi^\alpha + \theta^\alpha \eta^\alpha\big) \\ &\quad = \boldsymbol{\sigma} : \boldsymbol{l}_\alpha - \operatorname{div} \boldsymbol{q}^\alpha + \rho^\alpha r^\alpha + \hat{e}^\alpha + \hat{\gamma}^\alpha\Big(\frac{1}{2}\boldsymbol{v}_\alpha \cdot \boldsymbol{v}_\alpha - e^\alpha\Big) - \boldsymbol{h}^\alpha \cdot \boldsymbol{v}_\alpha \end{aligned} \tag{98}$$

Next, isolate the material time derivative on the phase entropy:

$$\begin{aligned} \rho^\alpha D_t^\alpha \eta^\alpha = \frac{1}{\theta^\alpha}\Big(&- \rho^\alpha \big[D_t^\alpha \psi^\alpha + \eta^\alpha D_t^\alpha \theta^\alpha\big] + \boldsymbol{\sigma}^\alpha : \boldsymbol{l}_\alpha - \operatorname{div} \boldsymbol{q}^\alpha + \rho^\alpha r^\alpha + \hat{e}^\alpha \\ &+ \hat{\gamma}^\alpha\Big[\frac{1}{2}\boldsymbol{v}_\alpha \cdot \boldsymbol{v}_\alpha - e^\alpha\Big] - \boldsymbol{h}^\alpha \cdot \boldsymbol{v}_\alpha\Big) \end{aligned} \tag{99}$$

Substitute this into the entropy balance, Eq. 96:

$$\begin{aligned} \sum_\alpha \frac{1}{\theta^\alpha}\Big(&\hat{\gamma}^\alpha \theta^\alpha \eta^\alpha - \rho^\alpha \big[D_t^\alpha \psi^\alpha + \eta^\alpha D_t^\alpha \theta^\alpha\big] + \boldsymbol{\sigma}^\alpha : \boldsymbol{l}_\alpha - \operatorname{div} \boldsymbol{q}^\alpha + \rho^\alpha r^\alpha + \hat{e}^\alpha \\ &+ \hat{\gamma}^\alpha\Big[\frac{1}{2}\boldsymbol{v}_\alpha \cdot \boldsymbol{v}_\alpha - e^\alpha\Big] - \boldsymbol{h}^\alpha \cdot \boldsymbol{v}_\alpha - \rho^\alpha r^\alpha + \theta^\alpha \operatorname{div}\Big[\frac{1}{\theta^\alpha}\boldsymbol{q}^\alpha\Big]\Big) \geq 0 \end{aligned} \tag{100}$$

Recognize that heat source/sink terms cancel such that the total dissipation inequal-

ity may be written as

$$\sum_{\alpha} \frac{1}{\theta^{\alpha}} \Big(\rho^{\alpha} \big[D_t^{\alpha} \psi^{\alpha} + \eta^{\alpha} D_t^{\alpha} \theta^{\alpha} \big] - \boldsymbol{\sigma}^{\alpha} : \boldsymbol{l}_{\alpha} - \hat{e}^{\alpha} + \hat{\gamma}^{\alpha} \Big[\psi^{\alpha} - \frac{1}{2} \boldsymbol{v}_{\alpha} \cdot \boldsymbol{v}_{\alpha} \Big] + \boldsymbol{h}^{\alpha} \cdot \boldsymbol{v}_{\alpha} + \frac{1}{\theta^{\alpha}} \mathrm{grad}(\theta^{\alpha}) \cdot \boldsymbol{q}^{\alpha} \Big) \geq 0 \tag{101}$$

Given the above summation over the mixture, iff $\theta^{\alpha} = \theta$ (i.e., mixed-temperature constituents), we write

$$\begin{aligned} \sum_{\alpha} \Big(& \rho^{\alpha} \big[D_t^{\alpha} \psi^{\alpha} + \eta^{\alpha} D_t^{\alpha} \theta^{\alpha} \big] - \boldsymbol{\sigma}^{\alpha} : \boldsymbol{l}_{\alpha} \\ & + \hat{\gamma}^{\alpha} \Big[\psi^{\alpha} - \frac{1}{2} \boldsymbol{v}_{\alpha} \cdot \boldsymbol{v}_{\alpha} \Big] + \boldsymbol{h}^{\alpha} \cdot \boldsymbol{v}_{\alpha} + \frac{1}{\theta} \mathrm{grad}(\theta) \cdot \boldsymbol{q}^{\alpha} \Big) \geq 0 \end{aligned} \tag{102}$$

where by definition the power density supply terms have cancelled with one another, and a constitutive relation for the local energy interaction term $\hat{\varepsilon}^{\alpha}$ is not needed. This is the strategy that is pursued herein.

If we were to naïvely multiply both sides of Eq. 101 by phase temperature under the admittedly reasonable assumption that temperature, being a positive quantity, would not change the sign of the dissipation inequality, then when carrying out the summation of the dissipation inequality over constituents $\alpha = \mathrm{s}, \mathrm{f}$, the power density supply terms would cancel. The issue with such a scenario is that if we were to later invoke the energy balance in Eq. 85 for any one phase, the local energy interaction term would not have been defined constitutively via the dissipation inequality. This is also the difficulty that arises when supposing that the second law need only be satisfied for an individual constituent. In that case, we might have written the dissipation inequality for each phase as follows (equation unnumbered since it is hypothetical):

$$\rho^{\alpha} \big[D_t^{\alpha} \psi^{\alpha} + \eta^{\alpha} D_t^{\alpha} \theta^{\alpha} \big] - \boldsymbol{\sigma}^{\alpha} : \boldsymbol{l}_{\alpha} - \hat{e}^{\alpha} + \hat{\gamma}^{\alpha} \Big[\psi^{\alpha} - \frac{1}{2} \boldsymbol{v}_{\alpha} \cdot \boldsymbol{v}_{\alpha} \Big] + \boldsymbol{h}^{\alpha} \cdot \boldsymbol{v}_{\alpha} + \frac{1}{\theta^{\alpha}} \mathrm{grad}(\theta)^{\alpha} \cdot \boldsymbol{q}^{\alpha} \geq 0$$

The power density supply terms $\hat{e}^{\alpha}$ would always cancel with one another when summing over phases here because they are not temperature scaled as in Eq. 101.

3. Constitutive Theory

3.1 Mixed-Temperature Model

In the mixed-temperature model, we may assume that there is no heat exchange between constituents in the mixture: $\theta^{\mathrm{s}} = \theta^{\mathrm{f}} = \theta$. Strictly speaking, this may not be an appropriate assumption for strong shocks; however, the analytical solution[23] for a strong compressive shock wave in air, when modeled as an ideal gas, shows that at 50% compression the pressure rise due to entropy production is only 7 kPa above the isentropic pressure of 178 kPa. Furthermore, Freed et al.[7] provided evidence that temperature fluctuations in lung parenchyma undergoing shock compression are minimal; rather, variance in elastic moduli give rise to larger fluctuations in deformation fields. Considering these, and that the kinematic balance relations become significantly more complex when multiphase temperatures are introduced (i.e., $\theta^{\mathrm{f}} \neq \theta^{\mathrm{s}}$), the current scope will assume a mixed temperature model (i.e., no heat exchange between the constituents).

By definition, for a closed system, that is, without supply from an external source,

$$\sum_{\alpha} \hat{\gamma}^{\alpha} = 0, \quad \sum_{\alpha} \boldsymbol{h}^{\alpha} = 0, \quad \sum_{\alpha} \hat{e}^{\alpha} = 0 \tag{103}$$

Then, using Eq. $103_{2,3}$ to group the interaction force terms and eliminate the phase power terms, the dissipation inequality may be written as

$$\begin{aligned} \rho^{\mathrm{s}}\left[D_t^{\mathrm{s}}\psi^{\mathrm{s}} + \eta^{\mathrm{s}} D_t^{\mathrm{s}}\theta\right] - \boldsymbol{\sigma}^{\mathrm{s}} : \boldsymbol{l}_{\mathrm{s}} + \frac{1}{\theta}\mathrm{grad}(\theta)\cdot(\boldsymbol{q}^{\mathrm{s}} + \boldsymbol{q}^{\mathrm{f}}) \\ + \rho^{\mathrm{f}}\left[D_t^{\mathrm{f}}\psi^{\mathrm{f}} + \eta^{\mathrm{f}} D_t^{\mathrm{f}}\theta\right] - \boldsymbol{\sigma}^{\mathrm{f}} : \boldsymbol{l}_{\mathrm{f}} + \boldsymbol{h}^{\mathrm{f}}\cdot\tilde{\boldsymbol{v}}_{\mathrm{f}} \geq 0 \end{aligned} \tag{104}$$

Following the approach of de Boer,[22] Ehlers,[20] Ghadiani,[72] and Markert,[73] we introduce the saturation constraint to the Clausius-Duhem inequality given by Eq. 104, namely,

$$n^{\mathrm{s}} + n^{\mathrm{f}} = 1, \quad D_t^{\mathrm{s}} n^{\mathrm{s}} + D_t^{\mathrm{s}} n^{\mathrm{f}} = 0 \tag{105}$$

which we can also express as

$$D_t^{\mathrm{s}} n^{\mathrm{s}} + D_t^{\mathrm{f}} n^{\mathrm{f}} - \mathrm{grad}(n^{\mathrm{f}})\cdot\tilde{\boldsymbol{v}}_{\mathrm{f}} = 0 \tag{106}$$

Utilization of the balance of mass,

$$\frac{n^\alpha}{\rho^{\alpha\mathrm{R}}} D_t^\alpha \rho^{\alpha\mathrm{R}} + D_t^\alpha n^\alpha + n^\alpha \operatorname{div} \boldsymbol{v}_\alpha = \frac{\hat{\gamma}^\alpha}{\rho^{\alpha\mathrm{R}}} \tag{107}$$

of each constituent (s) and (f) with assumption of negligible mass supplies, and incompressible solid (s) constituent, allows us to write the saturation constraint as

$$n^{\mathrm{s}} \operatorname{div} \boldsymbol{v}_{\mathrm{s}} + \frac{n^{\mathrm{f}}}{\rho^{\mathrm{fR}}} D_t^{\mathrm{f}} \rho^{\mathrm{fR}} + n^{\mathrm{f}} \operatorname{div} \boldsymbol{v}_{\mathrm{f}} + \operatorname{grad}(n^{\mathrm{f}}) \cdot \tilde{\boldsymbol{v}}_{\mathrm{f}} = 0 \tag{108}$$

The saturation constraint may be added to the Clausius-Duhem inequality, Eq. 104, with the introduction of a Lagrange multiplier $\mathcal{P}$, which will be identified later as excess pore fluid pressure:

$$\mathcal{P}\Big(n^{\mathrm{s}} \boldsymbol{d}_{\mathrm{s}} : \mathbf{1} + \frac{n^{\mathrm{f}}}{\rho^{\mathrm{fR}}} D_t^{\mathrm{f}} \rho^{\mathrm{fR}} + n^{\mathrm{f}} \boldsymbol{d}_{\mathrm{f}} : \mathbf{1} + \operatorname{grad}(n^{\mathrm{f}}) \cdot \tilde{\boldsymbol{v}}_{\mathrm{f}} \Big) = 0 \tag{109}$$

Adding this to the Clausius-Duhem inequality, and, combining terms and exploiting the symmetry of the partial Cauchy stress tensors, we may re-write the Clausius-Duhem inequality for the mixed-temperature case as

$$\begin{aligned} &\rho^{\mathrm{s}} D_t^{\mathrm{s}} \psi^{\mathrm{s}} + \rho^{\mathrm{f}} D_t^{\mathrm{f}} \psi^{\mathrm{f}} + \Big(\rho^{\mathrm{s}} \eta^{\mathrm{s}} \Big) D_t^{\mathrm{s}} \theta + \rho^{\mathrm{f}} \eta^{\mathrm{f}} D_t^{\mathrm{f}} \theta \\ &\quad - \Big(\big[\boldsymbol{\sigma}^{\mathrm{s}} + \mathcal{P} n^{\mathrm{s}} \mathbf{1} \big] : \boldsymbol{d}_{\mathrm{s}} + \big[\boldsymbol{\sigma}^{\mathrm{f}} + \mathcal{P} n^{\mathrm{f}} \mathbf{1} \big] : \boldsymbol{d}_{\mathrm{f}} \Big) \\ &\quad + (\boldsymbol{h}^{\mathrm{f}} - \mathcal{P} \operatorname{grad} n^{\mathrm{f}}) \cdot \tilde{\boldsymbol{v}}_{\mathrm{f}} + \frac{1}{\theta} \operatorname{grad}(\theta) \cdot (\boldsymbol{q}^{\mathrm{s}} + \boldsymbol{q}^{\mathrm{f}}) - \mathcal{P} \frac{n^{\mathrm{f}}}{\rho^{\mathrm{fR}}} D_t^{\mathrm{f}} \rho^{\mathrm{fR}} \geq 0 \end{aligned} \tag{110}$$

Introduce the so-called "extra" terms which we can define constitutively later,

$$\begin{aligned} \boldsymbol{\sigma}_E^{\mathrm{s}} &= \boldsymbol{\sigma}^{\mathrm{s}} + \mathcal{P} n^{\mathrm{s}} \mathbf{1}, \\ \boldsymbol{\sigma}_E^{\mathrm{f}} &= \boldsymbol{\sigma}^{\mathrm{f}} + \mathcal{P} n^{\mathrm{f}} \mathbf{1}, \\ \boldsymbol{h}_E^{\mathrm{f}} &= \boldsymbol{h}^{\mathrm{f}} - \mathcal{P} \operatorname{grad} n^{\mathrm{f}} \end{aligned} \tag{111}$$

and substitute back into Eq. 110:

$$\begin{aligned} &\rho^{\mathrm{s}} D_t^{\mathrm{s}} \psi^{\mathrm{s}} + \rho^{\mathrm{f}} D_t^{\mathrm{f}} \psi^{\mathrm{f}} + \rho^{\mathrm{s}} \eta^{\mathrm{s}} D_t^{\mathrm{s}} \theta + \rho^{\mathrm{f}} \eta^{\mathrm{f}} D_t^{\mathrm{f}} \theta - \Big(\boldsymbol{\sigma}_E^{\mathrm{s}} : \boldsymbol{d}_{\mathrm{s}} + \boldsymbol{\sigma}_E^{\mathrm{f}} : \boldsymbol{d}_{\mathrm{f}} \Big) \\ &\qquad + \boldsymbol{h}_E^{\mathrm{f}} \cdot \tilde{\boldsymbol{v}}_{\mathrm{f}} - \mathcal{P} \frac{n^{\mathrm{f}}}{\rho^{\mathrm{fR}}} D_t^{\mathrm{f}} \rho^{\mathrm{fR}} + \frac{1}{\theta} \operatorname{grad} \theta \cdot (\boldsymbol{q}^{\mathrm{s}} + \boldsymbol{q}^{\mathrm{f}}) \geq 0 \end{aligned} \tag{112}$$

3.1.1 Determination of the Helmholtz Free Energies

Discussion of how to formulate constitutive equations is discussed in detail by Coleman and Noll,[71] Marsden and Hughes,[74] and Truesdell,[75] and specifically for TPM by Truesdell and Toupin,[16] Ehlers,[20] and de Boer.[22] Following the approach of Ghadiani,[72] the following response functions $\mathcal{R}$ must be determined:

$$\mathcal{R} := \left\{ \psi^{\mathrm{s}}, \psi^{\mathrm{f}}, \boldsymbol{\sigma}^{\mathrm{s}}_E, \boldsymbol{\sigma}^{\mathrm{f}}_E, \boldsymbol{h}^{\mathrm{f}}_E, \boldsymbol{q}^{\mathrm{s}}, \boldsymbol{q}^{\mathrm{f}} \right\} \tag{113}$$

which depend on a set $\mathcal{S}$ of variables:

$$\mathcal{R} := \mathcal{R}(\mathcal{S}) \tag{114}$$

where $\mathcal{S}$ is a subset of the fundamental constitutive variables $\mathcal{V}$ for a biphasic continuum with an elastic solid constituent:

$$\mathcal{V} := \left\{ \theta^{\alpha}, \mathrm{grad}\theta^{\alpha}, n^{\mathrm{f}}, \mathrm{grad}n^{\mathrm{f}}, \rho^{\alpha\mathrm{R}}, \mathrm{grad}\rho^{\alpha\mathrm{R}}, \boldsymbol{F}_{\alpha}, \mathrm{GRAD}_{\alpha}\, \boldsymbol{F}_{\alpha}, \boldsymbol{v}_{\mathrm{f}}, \mathrm{GRAD}_{\mathrm{f}}\, \boldsymbol{v}_{\mathrm{f}}, \boldsymbol{X}_{\alpha} \right\} \tag{115}$$

For an isotropic pore fluid, the deformation gradient $\boldsymbol{F}_{\mathrm{f}}$ must have the form[76]

$$\boldsymbol{F}_{\mathrm{f}} = (\det \boldsymbol{F}_{\mathrm{f}})^{1/3} \mathbf{1} \tag{116}$$

and thus $\boldsymbol{F}_{\mathrm{f}}$ must be substituted by $\det \boldsymbol{F}_{\mathrm{f}}$, which can be determined through porosity n^{f} and real fluid mass density ρ^{fR} in the absence of fluid mass supply $\hat{\gamma}^{\mathrm{f}}$. Using the principle of frame indifference, we may also substitute the pore fluid velocity $\boldsymbol{v}_{\mathrm{f}}$ by the seepage velocity $\tilde{\boldsymbol{v}}_{\mathrm{f}}$. The pore fluid velocity gradient $\mathrm{GRAD}_{\mathrm{f}}\, \boldsymbol{v}_{\mathrm{f}}$ may also substituted by the deformation rate tensor $\boldsymbol{d}_{\mathrm{f}}$.

Furthermore, it can be shown through direct integration of Eq. 46 for $\alpha = \mathrm{s}$ and the incompressibility assumption, that porosity, solid (s) real mass density and its gradient, are all functions of deformation $\boldsymbol{F}_{\mathrm{s}}$, and thus they can be eliminated from the set of constitutive variables $\mathcal{S}$ such that

$$\mathcal{S} = \left\{ \theta, \mathrm{grad}\theta, \rho^{\mathrm{fR}}, \mathrm{grad}\rho^{\mathrm{fR}}, \boldsymbol{F}_{\mathrm{s}}, \mathrm{GRAD}_{\mathrm{s}}\, \boldsymbol{F}_{\mathrm{s}}, \tilde{\boldsymbol{v}}_{\mathrm{f}}, \boldsymbol{d}_{\mathrm{f}} \right\} \tag{117}$$

where we have also made use of $\theta^\alpha = \theta$. Combining Eqs. 113, 114, and 117,

$$\left\{\psi^{\mathrm{s}}, \psi^{\mathrm{f}}, \boldsymbol{\sigma}^{\mathrm{s}}_E, \boldsymbol{\sigma}^{\mathrm{f}}_E, \boldsymbol{h}^{\mathrm{f}}_E, \boldsymbol{q}^{\mathrm{s}}, \boldsymbol{q}^{\mathrm{f}}\right\} = \mathcal{R}(\theta, \mathrm{grad}\theta, \rho^{\mathrm{fR}}, \mathrm{grad}\rho^{\mathrm{fR}}, \boldsymbol{F}_{\mathrm{s}}, \mathrm{GRAD}_{\mathrm{s}}\, \boldsymbol{F}_{\mathrm{s}}, \tilde{\boldsymbol{v}}_{\mathrm{f}}, \boldsymbol{d}_{\mathrm{f}}) \tag{118}$$

Based on the principle of phase separation, that the Helmholtz free energy of constituent α should depend only on the α variables, we may write

$$\begin{aligned} \psi^{\mathrm{s}} &:= \psi^{\mathrm{s}}(\theta, \mathrm{grad}\theta, \boldsymbol{C}_{\mathrm{s}}, \mathrm{GRAD}_{\mathrm{s}}\, \boldsymbol{C}_{\mathrm{s}}), \\ \psi^{\mathrm{f}} &:= \psi^{\mathrm{f}}(\theta, \mathrm{grad}\theta, \rho^{\mathrm{fR}}, \mathrm{grad}\rho^{\mathrm{fR}}, \tilde{\boldsymbol{v}}_{\mathrm{f}}, \boldsymbol{d}_{\mathrm{f}}) \end{aligned} \tag{119}$$

where we have used the right Cauchy-Green tensor $\boldsymbol{C}_{\mathrm{s}} = \boldsymbol{F}_{\mathrm{s}}^T \boldsymbol{F}_{\mathrm{s}}$ in place of $\boldsymbol{F}_{\mathrm{s}}$. The material time derivatives of the Helmholtz free energy functions are

$$\begin{aligned} D^{\mathrm{s}}_t \psi^{\mathrm{s}} = \frac{\partial \psi^{\mathrm{s}}}{\partial \theta} D^{\mathrm{s}}_t \theta + \frac{\partial \psi^{\mathrm{s}}}{\partial (\mathrm{grad}\theta)} D^{\mathrm{s}}_t (\mathrm{grad}\theta) \\ + \frac{\partial \psi^{\mathrm{s}}}{\partial \boldsymbol{C}_{\mathrm{s}}} D^{\mathrm{s}}_t \boldsymbol{C}_{\mathrm{s}} + \frac{\partial \psi^{\mathrm{s}}}{\partial (\mathrm{GRAD}_{\mathrm{s}}\, \boldsymbol{C}_{\mathrm{s}})} D^{\mathrm{s}}_t (\mathrm{GRAD}_{\mathrm{s}}\, \boldsymbol{C}_{\mathrm{s}}) \end{aligned} \tag{120}$$

$$\begin{aligned} D^{\mathrm{f}}_t \psi^{\mathrm{f}} = \frac{\partial \psi^{\mathrm{f}}}{\partial \theta} D^{\mathrm{f}}_t \theta + \frac{\partial \psi^{\mathrm{f}}}{\partial (\mathrm{grad}\theta)} D^{\mathrm{f}}_t (\mathrm{grad}\theta) + \frac{\partial \psi^{\mathrm{f}}}{\partial \rho^{\mathrm{fR}}} D^{\mathrm{f}}_t \rho^{\mathrm{fR}} + \\ \frac{\partial \psi^{\mathrm{f}}}{\partial (\mathrm{grad}\rho^{\mathrm{fR}})} D^{\mathrm{f}}_t (\mathrm{grad}\rho^{\mathrm{fR}}) + \frac{\partial \psi^{\mathrm{f}}}{\partial \tilde{\boldsymbol{v}}_{\mathrm{f}}} D^{\mathrm{f}}_t \tilde{\boldsymbol{v}}_{\mathrm{f}} + \frac{\partial \psi^{\mathrm{f}}}{\partial \boldsymbol{d}_{\mathrm{f}}} D^{\mathrm{f}}_t \boldsymbol{d}_{\mathrm{f}} \end{aligned} \tag{121}$$

3.1.2 Evaluation of the Clausius-Duhem Inequality

Returning our attention to Eq. 112, we may substitute the material time derivatives of the Helmholtz free energy functions:

$$\begin{aligned}\Big(\rho^{\mathrm{s}}\frac{\partial\psi^{\mathrm{s}}}{\partial\theta}+\rho^{\mathrm{s}}\eta^{\mathrm{s}}\Big)D_t^{\mathrm{s}}\theta+\rho^{\mathrm{s}}\frac{\partial\psi^{\mathrm{s}}}{\partial(\mathrm{grad}\theta)}D_t^{\mathrm{s}}(\mathrm{grad}\theta)+\Big(\rho^{\mathrm{s}}\frac{\partial\psi^{\mathrm{s}}}{\partial\boldsymbol{C}_{\mathrm{s}}}-\frac{1}{2J_{\mathrm{s}}}\boldsymbol{S}_E^{\mathrm{s}}\Big):D_t^{\mathrm{s}}\boldsymbol{C}_{\mathrm{s}}\\ +\rho^{\mathrm{s}}\frac{\partial\psi^{\mathrm{s}}}{\partial(\mathrm{GRAD}_{\mathrm{s}}\,\boldsymbol{F}_{\mathrm{s}})}D_t^{\mathrm{s}}(\mathrm{GRAD}_{\mathrm{s}}\,\boldsymbol{F}_{\mathrm{s}})+\Big(\rho^{\mathrm{f}}\frac{\partial\psi^{\mathrm{f}}}{\partial\theta}+\rho^{\mathrm{f}}\eta^{\mathrm{f}}\Big)D_t^{\mathrm{f}}\theta\\ +\rho^{\mathrm{f}}\frac{\partial\psi^{\mathrm{f}}}{\partial(\mathrm{grad}\theta)}D_t^{\mathrm{f}}(\mathrm{grad}\theta)+\Big(\rho^{\mathrm{f}}\frac{\partial\psi^{\mathrm{f}}}{\partial\rho^{\mathrm{fR}}}-\mathcal{P}\frac{n^{\mathrm{f}}}{\rho^{\mathrm{fR}}}\Big)D_t^{\mathrm{f}}\rho^{\mathrm{fR}}\\ +\rho^{\mathrm{f}}\frac{\partial\psi^{\mathrm{f}}}{\partial(\mathrm{grad}\rho^{\mathrm{fR}})}D_t^{\mathrm{f}}(\mathrm{grad}\rho^{\mathrm{fR}})+\rho^{\mathrm{f}}\frac{\partial\psi^{\mathrm{f}}}{\partial\tilde{\boldsymbol{v}}_{\mathrm{f}}}D_t^{\mathrm{f}}\tilde{\boldsymbol{v}}_{\mathrm{f}}+\frac{\partial\psi^{\mathrm{f}}}{\partial\boldsymbol{d}_{\mathrm{f}}}D_t^{\mathrm{f}}\boldsymbol{d}_{\mathrm{f}}-\boldsymbol{\sigma}_E^{\mathrm{f}}:\boldsymbol{d}_{\mathrm{f}}\\ +\boldsymbol{h}_E^{\mathrm{f}}\cdot\tilde{\boldsymbol{v}}_{\mathrm{f}}+\frac{1}{\theta}\mathrm{grad}\theta\cdot(\boldsymbol{q}^{\mathrm{s}}+\boldsymbol{q}^{\mathrm{f}})\geq 0\end{aligned}\tag{122}$$

where we have used the identities

$$D_t^{\mathrm{s}}\boldsymbol{C}_{\mathrm{s}}=2\boldsymbol{F}_{\mathrm{s}}^T\boldsymbol{d}_{\mathrm{s}}\boldsymbol{F}_{\mathrm{s}},\quad \boldsymbol{\sigma}_E^{\mathrm{s}}=\frac{1}{J_{\mathrm{s}}}\boldsymbol{F}_{\mathrm{s}}\boldsymbol{S}_E^{\mathrm{s}}\boldsymbol{F}_{\mathrm{s}}^T\tag{123}$$

to transform the solid extra stress to the reference configuration of the solid skeleton.

Using the Coleman and Noll[71] argument, the following constitutive relations must

hold:

$$
\begin{aligned}
\left(\rho^{\mathrm{s}}\frac{\partial\psi^{\mathrm{s}}}{\partial\theta}+\rho^{\mathrm{s}}\eta^{\mathrm{s}}\right)=0 \;\Rightarrow \rho^{\mathrm{s}}_{0(\mathrm{s})}\eta^{\mathrm{s}}=-\frac{\partial(\rho^{\mathrm{s}}_{0(\mathrm{s})}\psi^{\mathrm{s}})}{\partial\theta},\\
\frac{\partial\psi^{\mathrm{s}}}{\partial(\mathrm{grad}\theta)}=0,\\
\left(\rho^{\mathrm{s}}\frac{\partial\psi^{\mathrm{s}}}{\partial\boldsymbol{C}_{\mathrm{s}}}\boldsymbol{C}_{\mathrm{s}}-\frac{1}{2J_{\mathrm{s}}}\boldsymbol{S}^{\mathrm{s}}_{E}\right)=\boldsymbol{0} \;\Rightarrow \boldsymbol{S}^{\mathrm{s}}_{E}=2\frac{\partial(\rho^{\mathrm{s}}_{0(\mathrm{s})}\psi^{\mathrm{s}})}{\partial\boldsymbol{C}_{\mathrm{s}}},\\
\frac{\partial\psi^{\mathrm{s}}}{\partial(\mathrm{GRAD}_{\mathrm{s}}\,\boldsymbol{C}_{\mathrm{s}})}=\boldsymbol{0},\\
\left(\rho^{\mathrm{f}}\frac{\partial\psi^{\mathrm{f}}}{\partial\theta}+\rho^{\mathrm{f}}\eta^{\mathrm{f}}\right)=0 \;\Rightarrow \eta^{\mathrm{f}}=-\frac{\partial\psi^{\mathrm{f}}}{\partial\theta},\\
\frac{\partial\psi^{\mathrm{f}}}{\partial(\mathrm{grad}\theta)}=0,\\
\left(\rho^{\mathrm{f}}\frac{\partial\psi^{\mathrm{f}}}{\partial\rho^{\mathrm{fR}}}-\mathcal{P}\frac{n^{\mathrm{f}}}{\rho^{\mathrm{fR}}}\right)=0 \;\Rightarrow \mathcal{P}=(\rho^{\mathrm{fR}})^2\frac{\partial\psi^{\mathrm{f}}}{\partial\rho^{\mathrm{fR}}},\\
\frac{\partial\psi^{\mathrm{f}}}{\partial(\mathrm{grad}\rho^{\mathrm{fR}})}=0,\\
\frac{\partial\psi^{\mathrm{f}}}{\partial\tilde{\boldsymbol{v}}_{\mathrm{f}}}=\boldsymbol{0},\\
\frac{\partial\psi^{\mathrm{f}}}{\partial\boldsymbol{d}_{\mathrm{f}}}=\boldsymbol{0}
\end{aligned}
\tag{124}
$$

and

$$
\mathcal{D}=\boldsymbol{\sigma}^{\mathrm{f}}_{E}:\boldsymbol{d}_{\mathrm{f}}-\boldsymbol{h}^{\mathrm{f}}_{E}\cdot\tilde{\boldsymbol{v}}_{\mathrm{f}}-\frac{1}{\theta}\mathrm{grad}(\theta)\cdot(\boldsymbol{q}^{\mathrm{s}}+\boldsymbol{q}^{\mathrm{f}})\geq 0 \tag{125}
$$

From Eq. 124, we can deduce that the Helmholtz free energy functions simplify to

$$
\begin{aligned}
\psi^{\mathrm{s}} &:= \psi^{\mathrm{s}}(\theta,\boldsymbol{C}_{\mathrm{s}}),\\
\psi^{\mathrm{f}} &:= \psi^{\mathrm{f}}(\theta,\rho^{\mathrm{fR}})
\end{aligned}
\tag{126}
$$

Given the dependence of solid entropy and stress on the solid Helmholtz free energy, we must have

$$
\begin{aligned}
\boldsymbol{\sigma}^{\mathrm{s}} &:= \boldsymbol{\sigma}^{\mathrm{s}}(\theta,\boldsymbol{C}_{\mathrm{s}}),\\
\eta^{\mathrm{s}} &:= \eta^{\mathrm{s}}(\theta,\boldsymbol{C}_{\mathrm{s}})
\end{aligned}
\tag{127}
$$

and analogously for the pore fluid,

$$\begin{aligned} \mathcal{P} &:= \mathcal{P}(\rho^{\mathrm{fR}}), \\ \eta^{\mathrm{f}} &:= \eta^{\mathrm{f}}(\theta, \rho^{\mathrm{fR}}) \end{aligned} \tag{128}$$

3.1.3 Identification of the Lagrange Multiplier

From thermodynamic principles (e.g., Davison,[61] Clayton[62,70]) for a compressible fluid with free energy as a function of specific volume v^{f} and temperature θ^{f}, we know that

$$\frac{\partial \psi^{\mathrm{f}}}{\partial v^{\mathrm{f}}} = -p_{\mathrm{f}} \Rightarrow \frac{\partial \psi^{\mathrm{f}}}{\partial \rho^{\mathrm{fR}}} \frac{\partial \rho^{\mathrm{fR}}}{\partial v^{\mathrm{f}}} = -p_{\mathrm{f}} \Rightarrow (\rho^{\mathrm{fR}})^2 \frac{\partial \psi^{\mathrm{f}}}{\partial \rho^{\mathrm{fR}}} = p_{\mathrm{f}} \tag{129}$$

Therefore by using Eq. 124_7, we see that the Lagrange multiplier $\mathcal{P}$ is identified as excess pore fluid pressure, such that the partial Cauchy stresses for each constituent are defined as

$$\begin{aligned} \boldsymbol{\sigma}^{\mathrm{s}} &= \boldsymbol{\sigma}^{\mathrm{s}}_E - p_{\mathrm{f}} n^{\mathrm{s}} \mathbf{1}, \\ \boldsymbol{\sigma}^{\mathrm{f}} &= \boldsymbol{\sigma}^{\mathrm{f}}_E - p_{\mathrm{f}} n^{\mathrm{f}} \mathbf{1} \end{aligned} \tag{130}$$

with

$$\boldsymbol{h}^{\mathrm{f}}_E = \boldsymbol{h}^{\mathrm{f}} - p_{\mathrm{f}} \mathrm{grad} n^{\mathrm{f}} \tag{131}$$

3.1.4 Identifying Constitutive Relations

From Eq. 125, we must find the following set of response functions for $\mathcal{D}$:

$$\left\{ \boldsymbol{\sigma}^{\mathrm{f}}_E, \hat{\varepsilon}^{\mathrm{f}}, \boldsymbol{h}^{\mathrm{f}}_E, \boldsymbol{q}^{\mathrm{s}}, \boldsymbol{q}^{\mathrm{f}} \right\} := \Upsilon(\mathcal{S}) \tag{132}$$

where

$$\mathcal{S} = \left\{ \theta, \mathrm{grad}\theta, \rho^{\mathrm{fR}}, \mathrm{grad}\rho^{\mathrm{fR}}, \boldsymbol{C}_{\mathrm{s}}, \mathrm{GRAD}_{\mathrm{s}} \boldsymbol{C}_{\mathrm{s}}, \tilde{\boldsymbol{v}}_{\mathrm{f}}, \boldsymbol{d}_{\mathrm{f}} \right\} \tag{133}$$

In order to identify the form of the response functions as they relate to the set of constitutive variables, we will expand $\mathcal{D}$ into equilibrium and non-equilibrium

parts:

$$\mathcal{D} = \mathcal{D}_0(\mathcal{S}_0) + \mathcal{D}_n(\mathcal{S}) \tag{134}$$

where

$$\mathcal{D}_0(\mathcal{S}) := 0; \quad \mathcal{D}(\mathcal{S}_0) := 0 \tag{135}$$

and the initial state is at thermal and mechanical equilibrium:

$$\begin{aligned} \mathcal{S}_0 = \{\theta = \theta_0, \mathrm{grad}\theta = \mathbf{0}, \rho^{\mathrm{fR}} = \rho_0^{\mathrm{fR}}, \mathrm{grad}\rho^{\mathrm{fR}} = \mathbf{0}, \boldsymbol{C}_{\mathrm{s}} = \mathbf{1}, \\ \mathrm{GRAD}_{\mathrm{s}}\, \boldsymbol{C}_{\mathrm{s}} = \mathbf{0}, \tilde{\boldsymbol{v}}_{\mathrm{f}} = \mathbf{0}, \boldsymbol{d}_{\mathrm{f}} = \mathbf{0}\} \end{aligned} \tag{136}$$

Thus, it follows that the response functions satisfy

$$\begin{aligned} \boldsymbol{\sigma}^{\mathrm{f}}_E(\mathcal{S}) &= \boldsymbol{\sigma}^{\mathrm{f}}_{E_n}(\mathcal{S}), \\ \boldsymbol{h}^{\mathrm{f}}_E(\mathcal{S}) &= \boldsymbol{h}^{\mathrm{f}}_{E_n}(\mathcal{S}), \\ \boldsymbol{q}^{\mathrm{s}}(\mathcal{S}) &= \boldsymbol{q}^{\mathrm{s}}_n(\mathcal{S}), \\ \boldsymbol{q}^{\mathrm{f}}(\mathcal{S}) &= \boldsymbol{q}^{\mathrm{f}}_n(\mathcal{S}) \end{aligned} \tag{137}$$

Next, we make the following constitutive assumptions about the functional dependencies of the response functions. The pore fluid extra stress $\boldsymbol{\sigma}^{\mathrm{f}}_E$ is identified as the fluid frictional stress for a single-phase fluid, and, assuming a Newtonian fluid law, it is directly related to the pore fluid deformation rate tensor $\boldsymbol{d}_{\mathrm{f}}$. The heat fluxes $\boldsymbol{q}^{\mathrm{s}}$ and $\boldsymbol{q}^{\mathrm{f}}$ are assumed to depend only on the mixture temperature gradient via Fourier's law. Lastly, the interaction term $\boldsymbol{h}^{\mathrm{f}}_E$ depends on the interaction variable $\tilde{\boldsymbol{v}}_{\mathrm{f}}$ (the seepage velocity). In other words,

$$\begin{aligned} \boldsymbol{\sigma}^{\mathrm{f}}_E &:= \boldsymbol{\sigma}^{\mathrm{f}}_E(\boldsymbol{d}_{\mathrm{f}}), \\ \boldsymbol{h}^{\mathrm{f}}_E &:= \boldsymbol{h}^{\mathrm{f}}_E(\tilde{\boldsymbol{v}}_{\mathrm{f}}), \\ \boldsymbol{q}^{\mathrm{s}} &:= \boldsymbol{q}^{\mathrm{s}}(\theta), \\ \boldsymbol{q}^{\mathrm{f}} &:= \boldsymbol{q}^{\mathrm{f}}(\theta) \end{aligned} \tag{138}$$

which leads to the following linearizations of the response functions using a Taylor series expansion around $\mathcal{S}_0$ and neglecting higher order terms:

$$\begin{aligned}
\boldsymbol{\sigma}^{\mathrm{f}}_{E_n}(\mathcal{S}) &= \boldsymbol{\sigma}^{\mathrm{f}}_{E_0} + \frac{\partial \boldsymbol{\sigma}^{\mathrm{f}}_{E_n}}{\partial \boldsymbol{d}_{\mathrm{f}}}\Big|_{\mathcal{S}_0} \boldsymbol{d}_{\mathrm{f}}, \\
\boldsymbol{h}^{\mathrm{f}}_{E_n}(\mathcal{S}) &= \boldsymbol{h}^{\mathrm{f}}_{E_0} + \frac{\partial \boldsymbol{h}^{\mathrm{f}}_{E_n}}{\partial \tilde{\boldsymbol{v}}_{\mathrm{f}}}\Big|_{\mathcal{S}_0} \tilde{\boldsymbol{v}}_{\mathrm{f}}, \\
\boldsymbol{q}^{\mathrm{s}}_{n}(\mathcal{S}) &= \boldsymbol{q}^{\mathrm{s}}_{0} + \frac{\partial \boldsymbol{q}^{\mathrm{s}}}{\partial (\mathrm{grad}\theta)}\Big|_{\mathcal{S}_0} \mathrm{grad}\theta, \\
\boldsymbol{q}^{\mathrm{f}}_{n}(\mathcal{S}) &= \boldsymbol{q}^{\mathrm{f}}_{0} + \frac{\partial \boldsymbol{q}^{\mathrm{f}}}{\partial (\mathrm{grad}\theta)}\Big|_{\mathcal{S}_0} \mathrm{grad}\theta
\end{aligned} \tag{139}$$

It is assumed that the initial values of the response functions are zero based on Eq. 136, such that the Taylor series expansion simplifies to

$$\begin{aligned}
\boldsymbol{\sigma}^{\mathrm{f}}_{E_n}(\mathcal{S}) &= \overset{4}{\boldsymbol{Z}}_{\mathrm{f}} \boldsymbol{d}_{\mathrm{f}}, \\
\boldsymbol{h}^{\mathrm{f}}_{E_n}(\mathcal{S}) &= \boldsymbol{S}_w \tilde{\boldsymbol{v}}_{\mathrm{f}}, \\
\boldsymbol{q}^{\mathrm{s}}_{n}(\mathcal{S}) &= \boldsymbol{k}^{\theta^{\mathrm{s}}} \mathrm{grad}\theta, \\
\boldsymbol{q}^{\mathrm{f}}_{n}(\mathcal{S}) &= \boldsymbol{k}^{\theta^{\mathrm{f}}} \mathrm{grad}\theta
\end{aligned} \tag{140}$$

where we have defined

$$\begin{aligned}
\overset{4}{\boldsymbol{Z}}_{\mathrm{f}} &:= \frac{\partial \boldsymbol{\sigma}^{\mathrm{f}}_{E_n}}{\partial \boldsymbol{d}_{\mathrm{f}}}\Big|_{\mathcal{S}_0}, \\
\boldsymbol{S}_w &:= \frac{\partial \boldsymbol{h}^{\mathrm{f}}_{E_n}}{\partial \tilde{\boldsymbol{v}}_{\mathrm{f}}}\Big|_{\mathcal{S}_0}, \\
\boldsymbol{k}^{\theta^{\mathrm{s}}} &:= \frac{\partial \boldsymbol{q}^{\mathrm{s}}}{\partial (\mathrm{grad}\theta)}\Big|_{\mathcal{S}_0}, \\
\boldsymbol{k}^{\theta^{\mathrm{f}}} &:= \frac{\partial \boldsymbol{q}^{\mathrm{s}}}{\partial (\mathrm{grad}\theta)}\Big|_{\mathcal{S}_0}
\end{aligned} \tag{141}$$

Thus the reduced dissipation inequality, Eq. 125, becomes

$$\mathcal{D} = (\overset{4}{\boldsymbol{Z}}_{\mathrm{f}} \boldsymbol{d}_{\mathrm{f}}) : \boldsymbol{d}_{\mathrm{f}} - (\boldsymbol{S}_w \tilde{\boldsymbol{v}}_{\mathrm{f}}) \cdot \tilde{\boldsymbol{v}}_{\mathrm{f}} - \frac{\mathrm{grad}(\theta)}{\theta}\Big(\mathrm{grad}(\theta) \cdot (\boldsymbol{k}^{\theta^{\mathrm{s}}} + \boldsymbol{k}^{\theta^{\mathrm{f}}})\Big) \geq 0 \tag{142}$$

To satisfy the inequality, each term must be non-negative by itself, and thus the following restrictions must hold:

$$\begin{aligned} \overset{4}{\boldsymbol{Z}}_{\mathrm{f}} &\rightarrow \text{ positive definite}, \\ -\boldsymbol{S}_w &\rightarrow \text{ positive definite}, \\ -\boldsymbol{k}^{\theta^{\mathrm{s}}} &\rightarrow \text{ positive definite}, \\ -\boldsymbol{k}^{\theta^{\mathrm{f}}} &\rightarrow \text{ positive definite} \end{aligned} \tag{143}$$

Substitution of Eq. 143 back into Eq. 140 gives,

$$\begin{aligned} \boldsymbol{\sigma}_E^{\mathrm{f}} &= \overset{4}{\boldsymbol{Z}}_{\mathrm{f}} \boldsymbol{d}_{\mathrm{f}}, \\ \boldsymbol{h}_E^{\mathrm{f}} &= -\boldsymbol{S}_w \tilde{\boldsymbol{v}}_{\mathrm{f}}, \\ \boldsymbol{q}^{\mathrm{s}} &= -\boldsymbol{k}^{\theta^{\mathrm{s}}} \mathrm{grad}\theta, \\ \boldsymbol{q}^{\mathrm{f}} &= -\boldsymbol{k}^{\theta^{\mathrm{f}}} \mathrm{grad}\theta \end{aligned} \tag{144}$$

3.1.5 Defining Proportionality Parameters

A common choice for the fourth-order tensor $\boldsymbol{Z}_{\mathrm{f}}$ is a simple Newtonian fluid law (see Holzapfel[69] p. 203):

$$\overset{4}{\boldsymbol{Z}}_{\mathrm{f}} := n^{\mathrm{f}} \kappa_{\mathrm{f}} (\mathbf{1} \otimes \mathbf{1}) + 2 n^{\mathrm{f}} \eta_{\mathrm{f}} (\mathbf{1} \otimes \mathbf{1})^{\overset{23}{T}} \tag{145}$$

where κ_{f} and η_{f} are the bulk and shear viscosity of the pore fluid, respectively.

When determining the form of $\boldsymbol{k}^{\theta^{\alpha}}$, we may assume isotropic heat conduction for simplicity such that

$$\boldsymbol{k}^{\theta^{\alpha}} = \begin{bmatrix} k^{\theta^{\alpha}} & 0 & 0 \\ 0 & k^{\theta^{\alpha}} & 0 \\ 0 & 0 & k^{\theta^{\alpha}} \end{bmatrix} (\boldsymbol{e}_i \otimes \boldsymbol{e}_j) \tag{146}$$

$$\tag{147}$$

The permeability tensor $\boldsymbol{S}_w$ may be defined as

$$\boldsymbol{S}_w := (n^{\mathrm{f}})^2 (\boldsymbol{K}^{\mathrm{s}})^{-1} = \frac{(n^{\mathrm{f}})^2}{\hat{k}} \mathbf{1} \tag{148}$$

where $\boldsymbol{K}^{\mathrm{s}}$ is the intrinsic permeability of the solid skeleton, which we have also taken to be isotropic for sake of simplicity, and $\hat{k}$ is the hydraulic conductivity defined as

$$\hat{k} := \frac{\varkappa}{\eta_{\mathrm{f}}} \frac{\mathcal{F}\left(n^{\mathrm{f}}\right)}{\mathcal{F}\left(n_0^{\mathrm{f}}\right)} \tag{149}$$

where $\varkappa$ is the intrinsic permeability of the solid skeleton (units of m^{-2}), and $\mathcal{F}$ is a nonlinear function of porosity n^{f} accounting for change in hydraulic permeability due to change in porosity (e.g., the Kozeny-Carman relation):

$$\mathcal{F}\left(n^{\mathrm{f}}\right) := \frac{\left(n^{\mathrm{f}}\right)^3}{1-\left(n^{\mathrm{f}}\right)^2} \tag{150}$$

Recall that

$$\boldsymbol{h}_E^{\mathrm{f}} := \boldsymbol{h}^{\mathrm{f}} - p_{\mathrm{f}} \mathrm{grad} n^{\mathrm{f}} \tag{151}$$

Following this, we may use the balance of momentum, Eq. 53, for $\alpha = \mathrm{f}$ and taking $\hat{\gamma}^{\mathrm{f}} = 0$ and $\boldsymbol{b}^{\mathrm{f}} = \boldsymbol{b}^{\mathrm{s}} = \boldsymbol{b}$, and Eq. 130_2 to substitute the term $\boldsymbol{h}^{\mathrm{f}} - p_{\mathrm{f}} \mathrm{grad} n^{\mathrm{f}}$ in Eq. 151, such that

$$\boldsymbol{h}_E^{\mathrm{f}} = \rho^{\mathrm{f}}(\boldsymbol{a}_{\mathrm{f}} - \boldsymbol{b}^{\mathrm{f}}) - \operatorname{div} \boldsymbol{\sigma}_E^{\mathrm{f}} + n^{\mathrm{f}} \mathrm{grad} p_{\mathrm{f}} \tag{152}$$

Then we may establish a generalized Darcy's law by substitution of Eq. 152 into Eq. 144_3 using the definition for $\boldsymbol{S}_w$ in Eq. 148:

$$n^{\mathrm{f}} \tilde{\boldsymbol{v}}_{\mathrm{f}} = -\hat{k}\left(\rho^{\mathrm{fR}}(\boldsymbol{a}_{\mathrm{f}} - \boldsymbol{b}) + \mathrm{grad} p_{\mathrm{f}} - \frac{1}{n^{\mathrm{f}}} \operatorname{div} \boldsymbol{\sigma}_E^{\mathrm{f}}\right) \tag{153}$$

Often, we choose to ignore the pore fluid extra stress such that $\boldsymbol{\sigma}_E^{\mathrm{f}} \approx \mathbf{0}$; this is what is meant when the pore fluid is assumed to be nearly-inviscid. The hydraulic conductivity, $\hat{k}$, is still associated with pore fluid viscosity (see Eq. 149). In this case, Eq. 153 simplifies to Eq. 60.

In the event that adiabatic conditions are assumed, then, for high rate loading pertinent to stress waves, including shocks, it is more convenient to work with an internal energy formulation than a free energy formulation.[23,62] Shock wave propagation is neither isentropic nor isothermal. Legendre transformations can be used to replace Eq. $124_{1,3,5,7}$ with constitutive equations in terms of internal energy functionals e^{α}. First, assume a functional dependence of internal energy and temperature of each phase as

$$(\rho^{\mathrm{s}}_{0(\mathrm{s})}e^{\mathrm{s}}) = (\rho^{\mathrm{s}}_{0(\mathrm{s})}e^{\mathrm{s}})(\boldsymbol{C}_{\mathrm{s}}, \eta^{\mathrm{s}}), \quad \theta = \theta(\boldsymbol{C}_{\mathrm{s}}, \eta^{\mathrm{s}}), \quad e^{\mathrm{f}} = e^{\mathrm{f}}(\rho^{\mathrm{fR}}, \eta^{\mathrm{f}}), \quad \theta = \theta(\rho^{\mathrm{fR}}, \eta^{\mathrm{f}}) \tag{154}$$

Then, chain-rule differentiation of Eq. 154 in combination with Eqs. $124_{1,3,5,7}$ and Eq. 129 leads to the following constitutive relations:

$$\begin{aligned} \theta &= \frac{1}{\rho^{\mathrm{s}}_{0(\mathrm{s})}} \frac{\partial(\rho^{\mathrm{s}}_{0(\mathrm{s})}e^{\mathrm{s}})}{\partial \eta^{\mathrm{s}}_{E}} = \frac{\partial e^{\mathrm{f}}}{\partial \eta^{\mathrm{f}}}, \\ \boldsymbol{S}^{\mathrm{s}}_{E} &= 2\frac{\partial(\rho^{\mathrm{s}}_{0(\mathrm{s})}e^{\mathrm{s}})}{\partial \boldsymbol{C}_{\mathrm{s}}}, \\ p_{\mathrm{f}} &= (\rho^{\mathrm{fR}})^2 \frac{\partial e^{\mathrm{f}}}{\partial \rho^{\mathrm{fR}}} \end{aligned} \tag{155}$$

Thus, only one constituent's internal energy function is sufficient to describe the temperature of the mixture if that constituent's entropy can be determined from the corresponding energy balance.

3.2.1 Hyperelastic Solid Skeleton

Oftentimes it is easier to constitutively define the solid skeleton stress (i.e., the solid extra stress) in terms of the symmetric second Piola-Kirchhoff effective stress $\boldsymbol{S}^{\mathrm{s}}_{E}$ which is what follows herein. However, for future numerical implementation, we convert one reference leg to the current configuration and use the first Piola-Kirchhoff stress via

$$\boldsymbol{P}^{\mathrm{s}}_{E} = \boldsymbol{F}_{\mathrm{s}}\boldsymbol{S}^{\mathrm{s}}_{E} \tag{156}$$

One of the most common strain-energy functionals for modeling nonlinear elastic materials undergoing large deformations is the neo-Hookean elastic strain-energy

functional:

$$W^{\mathrm{s}}(\boldsymbol{C}_{\mathrm{s}}, J_{\mathrm{s}}(\boldsymbol{C}_{\mathrm{s}})) = \frac{1}{2}\lambda(\ln J_{\mathrm{s}})^2 - \mu(\ln J_{\mathrm{s}}) + \frac{1}{2}\mu(\mathrm{tr}\,\boldsymbol{C}_{\mathrm{s}} - 3) \tag{157}$$

The solid skeleton isentropic Lamé parameters are μ and $\lambda := K^{\mathrm{skel}} - \frac{2}{3}\mu$. Thus, the internal energy function for the solid skeleton may be written as

$$(\rho^{\mathrm{s}}_{0(\mathrm{s})} e^{\mathrm{s}})(\boldsymbol{C}_{\mathrm{s}}, \eta^{\mathrm{s}}_E) := W^{\mathrm{s}}(\boldsymbol{C}_{\mathrm{s}}, J_{\mathrm{s}}(\boldsymbol{C}_{\mathrm{s}})) + \rho^{\mathrm{s}}_{0(\mathrm{s})}\theta_0(\eta^{\mathrm{s}} - \eta^{\mathrm{s}}_0)\Big[1 - \gamma^{\mathrm{s}} \ln J_{\mathrm{s}} + \frac{\eta^{\mathrm{s}} - \eta^{\mathrm{s}}_0}{2c^{\mathrm{s}}_V}\Big] \tag{158}$$

Thermoelastic coupling is invoked via the inclusion of a constant Grüneisen parameter of the solid γ^{s}, and c^{s}_V is the specific heat of the solid at constant volume per unit mass. The mixture temperature and second Piola effective stress are then, from Eq. $155_{1,2}$,

$$\begin{aligned} \theta \quad &= \theta^{\mathrm{s}}_0\Big[1 - \gamma^{\mathrm{s}} \ln J_{\mathrm{s}} + \frac{\eta_E - \eta^{\mathrm{s}}_0}{c^{\mathrm{s}}_V}\Big], \\ \boldsymbol{S}^{\mathrm{s}}_E \quad &= \mu\mathbf{1} + (\lambda \ln J_{\mathrm{s}} - \mu - \rho^{\mathrm{s}}_{0(\mathrm{s})}\theta^{\mathrm{s}}_0\gamma^{\mathrm{s}}[\eta^{\mathrm{s}}_E - \eta^{\mathrm{s}}_{E0}])\boldsymbol{C}^{-1}_{\mathrm{s}} \end{aligned} \tag{159}$$

In Eq. 159, thermo-mechanical coupling can be neglected by assuming $\gamma^{\mathrm{s}} \to 0$. This is assumed herein, as a non-zero Grüneisen parameter would allow for *thermal* compressibility of the solid, violating an earlier assumption that $D^{\mathrm{s}}_t \rho^{\mathrm{sR}} := 0$. The Grüneisen parameter for the solid skeleton of the lung parenchyma was calculated to be negligibly small in prior research,[14,23,77] supporting its omission in the current work.

3.2.2 Pore Fluid

The following form for the internal energy of the pore fluid is assumed,

$$e^{\mathrm{f}}(\rho^{\mathrm{fR}}, \eta^{\mathrm{f}}) := -\frac{1}{\rho^{\mathrm{fR}}}\Big[K^{\eta}_{\mathrm{f}} \ln\Big(\frac{\rho^{\mathrm{fR}}}{\rho^{\mathrm{fR}}_0}\Big) + K^{\eta}_{\mathrm{f}} + p_{\mathrm{f0}}\Big] + \theta_0\Big[(\eta^{\mathrm{f}} - \eta^{\mathrm{f}}_0) + \frac{(\eta^{\mathrm{f}} - \eta^{\mathrm{f}}_0)^2}{2c^{\mathrm{f}}_V}\Big] \tag{160}$$

where p_{f0} is the fluid pressure at reference density ρ^{fR}_0 and recalling K^{η}_{f} is the isentropic bulk modulus of the fluid. The reference entropy per unit mass, and specific heat at constant volume per unit mass of the fluid are η^{f}_0, and c^{f}_V. Applying

Eqs. $155_{3,4}$ allows us to derive the pressure-density and temperature-entropy as

$$\begin{aligned} p_{\mathrm{f}} &= K_{\mathrm{f}}^{\eta} \ln(\rho^{\mathrm{fR}}/\rho_0^{\mathrm{fR}}) + p_{\mathrm{f0}} \quad \Rightarrow \quad \rho^{\mathrm{fR}} = \rho_0^{\mathrm{fR}} \exp\left[(p_{\mathrm{f}} - p_{\mathrm{f0}})/K_{\mathrm{f}}^{\eta}\right], \\ \theta &= \theta_0[1 + (\eta^{\mathrm{f}} - \eta_0^{\mathrm{f}})/c_V^{\mathrm{f}}] \end{aligned} \tag{161}$$

Applying the D_t^{f} operation to Eq. 161_1 with $K_{\mathrm{f}}^{\eta} =$ constant produces Eq. 49.

3.2.3 A Note on Neglecting Thermomechanical Coupling

Because stresses (including pressures) and entropies are decoupled in the constitutive equations, the governing equations of momentum and mass conservation are unaffected by entropy or temperature fields. The computational implementation and results in related[68] and later works[65,66] focus on mechanical phenomena, whereby entropies, temperatures, and free and internal energy densities of phases need never be calculated explicitly. Dissipation and temperature changes, including possible heat conduction, can all still take place, but the thermal variables are not calculated in the forthcoming simulations since they do not affect the mechanical solutions. Accordingly, there is no need to prescribe values of specific heat capacities or thermal conductivities of phases.

In principle, an equation for the entropy rate of each phase can be obtained from manipulation of Eq. 85, but this derivation is not undertaken herein since entropy does not affect the mechanical fields of current focus. Future work will extend Eqs. 158 and 160 to include full stress-entropy and temperature-deformation couplings via inclusion of local energy interactions. Refer to Ghadiani[72] for an example of this, using a neo-Hookean model for the solid (s) constituent and the ideal gas law for the pore fluid (f) constituent.

4. Conclusions

We have presented a finite-strain framework of a biphasic mixture (i.e., coupled pore fluid flow and solid skeleton deformation) of a soft porous material (i.e., lung parenchyma) for high strain-rate dynamic loading. Our constitutive theory was nonlinear elastic and accounted for the compressibility of the pore air. The formulation herein did not make assumptions regarding the equivalency of acceleration of pore fluid to that of solid skeleton, but rather allowed them to be different. Furthermore, by use of the solid extra stress,[20,70] we were able to distinguish between solid skeleton, pore fluid (air) and total pressures, and stresses. Such metrics are important for understanding how damage from shock waves, or other impact events (e.g., blunt trauma from sports injury or vehicular collisions), will propagate through the porous lung tissue.

While the focus here was primarily on the deformation response of lung parenchyma, the general framework developed can be extended to measure the deformation response of other soft porous biological tissues (e.g., the brain), and, more broadly, other soft porous materials such as foams. Subsequent reports[65,66] address numerical implementation of the theory in a 1-D FE context and simulations of shock waves through the tissue-air mixture.

5. References

1. Cooper G, Townend D, Cater S, Pearce B. The role of stress waves in thoracic visceral injury from blast loading: Modification of stress transmission by foams and high-density materials. Journal of Biomechanics. 1991;24:273-285.

2. Cooper G. Protection of the lung from blast overpressure by thoracic stress wave decouplers. The Journal of Trauma: Injury, Infection, and Critical Care. 1996;40:105S-110S.

3. Tsokos M, Paulsen F, Petri S, Madea B, Püschel K, Türk E. Histologic, immunohistochemical, and ultrastructural findings in human blast lung injury. American Journal of Respiratory and Critical Care Medicine. 2003;168:549-555.

4. Cohn S, DuBose J. Pulmonary contusion: An update on recent advances in clinical management. World Journal of Surgery. 2010;34:1959-1970.

5. Clayton J, Freed A. A continuum mechanical model of the lung. DEVCOM Army Research Laboratory (US); 2019. Report No.: ARL-TR-8859.

6. Clayton J. Modeling lung tissue dynamics and injury under pressure and impact loading. Biomechanics and Modeling in Mechanobiology. 2020;19:2603-2626.

7. Freed A, Zamana S, Paul S, Clayton J. A dodecahedral model for alveoli. Part I. theory and numerical methods. DEVCOM Army Research Laboratory (US); 2021. Report No.: ARL-TR-9148.

8. Brannen M, Kang G, Dutrisac S, Banton R, Clayton J, Petel O. The influence of the tertiary bronchi on dynamic lung deformation. Journal of the Mechanical Behavior of Biomedical Materials. 2022;130:105181.

9. Sobin S, Fung Y, Tremer H. Collagen and elastin fibers in human pulmonary alveolar walls. Journal of Applied Physiology. 1988;64:1659-1675.

10. Suki B, Ito S, Stamenović D, Lutchen K, Ingenito E. Biomechanics of the lung parenchyma: critical roles of collagen and mechanical forces. Journal of Applied Physiology. 2005;98:1892-1899.

11. Suki B, Bates J. Lung tissue mechanics as an emergent phenomenon. Journal of Applied Physiology. 2011;110:1111-1118.

12. Clayton J, Banton R, Freed A. A nonlinear thermoelastic-viscoelastic continuum model of lung mechanics for shock wave analysis. In: Shock Compression of Condensed Matter; Vol. 2272. Lane J, editor. AIP Conference Proceedings; 2020. p. 040001.

13. Clayton JD, Freed AD. A constitutive model for lung mechanics and injury applicable to static, dynamic, and shock loading. Mechanics of Soft Materials. 2020;2.

14. Clayton J, Banton R, Goertz A. A continuum model of the human lung: Implementation and parameterization. DEVCOM Army Research Laboratory (US); 2021. Report No.: ARL-TR-9138.

15. Freed A, Clayton J. Coordinate indexing strategies for the laplace stretch in two and three dimensions. DEVCOM Army Research Laboratory (US); 2022. Report No.: ARL-TR-9530.

16. Truesdell C, Toupin R. The classical field theories. In: Handbuch der Physik; Vol. III. Flugge S, editor. Springer; 1960. p. 226–793.

17. Bowen R. Theory of mixtures. In: Continuum Physics; Vol. 3. Eringen A, editor. Academic Press; 1976. p. 1–127.

18. Bowen R. Incompressible porous media models by use of the theory of mixtures. International Journal of Engineering Science. 1980;18:1129–1148.

19. Bowen R. Compressible porous media models by use of the theory of mixtures. International Journal of Engineering Science. 1982;20:697–735.

20. Ehlers W. Foundations of multiphasic and porous materials. In: Porous media: theory, experiments and numerical applications. Ehlers W, Bluhm J, editors. Springer; 2002. p. 3–86.

21. Coussy O. Poromechanics. John Wiley and Sons; 2004.

22. de Boer R. Trends in continuum mechanics of porous media: Theory and applications of transport in porous media. Springer; 2005.

23. Clayton J. Analysis of shock waves in a mixture theory of a thermoelastic solid and fluid with distinct temperatures. International Journal of Engineering Science. 2022;175:103675.

24. Bowen R, Wright T. On the growth and decay of wave fronts in a mixture of linear elastic materials. Rendiconti del Circolo Matematico di Palermo. 1972;21:209–234.

25. Bowen R, Wright T. On wave propagation in a mixture of linear elastic materials. US Army Ballistic Research Laboratory; 1972. Report No.: 1581.

26. Lewis R, Schrefler B. The finite element method in the deformation and consolidation of porous media. John Wiley and Sons; 1987.

27. Schanz M. Poroelastodynamics: Linear models, analytical solutions, and numerical methods. Applied Mechanics Reviews. 2009;62:030803-1-030803-15.

28. Markert B, Heider Y, Ehlers W. Comparison of monolithic and splitting solution schemes for dynamic porous media problems. International Journal for Numerical Methods in Engineering. 2009;82:1341-1383.

29. Heider Y. Saturated porous media dynamics with application to earthquake engineering [thesis]. Institut für Mechanik (Bauwesen) Lehrstuhl für Kontinuumsmechanik; 2012 OCLC: 824646288.

30. Zienkiewicz O, Huang M, Wu J, Wu S. A new algorithm for the coupled soil–pore fluid problem. Shock and Vibration. 1993;1:3–14.

31. Li L, Zhou S, Du X, Song J, Gao C. Numerical study on the seismic response of fluid-saturated porous media using the precise time integration method. Applied Sciences. 2019;9:2037.

32. Li C, Borja R, Regueiro R. Dynamics of porous media at finite strain. Computer Methods in Applied Mechanics and Engineering. 2004;193:3837–3870.

33. Gajo A, Denzer R. Finite element modelling of saturated porous media at finite strains under dynamic conditions with compressible constituents. International Journal for Numerical Methods in Engineering. 2011;85:1705-1736.

34. Regueiro R, Zhang B, Wozniak S. Large deformation dynamic three-dimensional coupled finite element analysis of soft biological tissues treated

as biphasic porous media. Computer Modeling in Engineering and Sciences. 2014;98:1-39.

35. Zienkiewicz OC, Shiomi T. Dynamic behaviour of saturated porous media; the generalized Biot formulation and its numerical solution. International Journal for Numerical and Analytical Methods in Geomechanics. 1984;8:71-96.

36. Gajo A, Saetta A, Vitaliani R. Evaluation of three- and two-field finite element methods for the dynamic response of saturated soil. International Journal for Numerical Methods in Engineering. 1994;37:1231-1247.

37. Levenston ME, Frank EH, Grodzinsky AJ. Variationally derived 3-field finite element formulations for quasistatic poroelastic analysis of hydrated biological tissues. Computer Methods in Applied Mechanics and Engineering. 1998;156:231–246.

38. Yang Z. Poroviscoelastic dynamic finite element model of biological tissue [thesis]. University of Pittsburgh; 2006.

39. Lotfian Z, Sivaselvan M. Mixed finite element formulation for dynamics of porous media: Dynamics of porous media. International Journal for Numerical Methods in Engineering. 2018;115:141–171.

40. Wu W, Zheng H, Yang Y. Numerical manifold method for dynamic consolidation of saturated porous media with three-field formulation. International Journal for Numerical Methods in Engineering. 2019;120:768-802.

41. Zhang Y, Pedroso D, Li L, Scheuermann A, Ehlers W. Accurate and stabilised time integration strategy for saturated porous media dynamics. Acta Geotechnica. 2019;15:1859-1879.

42. Berger L. A low order finite element method for poroelasticity with applications to lung modelling [thesis]. University of Oxford; 2015.

43. Cao T, Sanavia L, Schrefler B. A thermo-hydro-mechanical model for multiphase geomaterials in dynamics with application to strain localization simulation. International Journal for Numerical Methods in Engineering. 2016;107:312–337.

44. Chapelle D, Moireau P. General coupling of porous flows and hyperelastic formulations – From thermodynamics principles to energy balance and compatible time schemes. European Journal of Mechanics. 2014;46:82-96.

45. Burtschell B, Chapelle D, Moireau P. Effective and energy-preserving time discretization for a general nonlinear poromechanical formulation. Computers and Structures. 2017;182:313–324.

46. Patte C, Genet M, Chapelle D. A quasi-static poromechanical model of the lungs. Biomechanics and Modeling in Mechanobiology. 2022;21:527–551.

47. Concha F, Hurtado D. Upscaling the poroelastic behavior of the lung parenchyma: A finite-deformation micromechanical model. Journal of the Mechanics and Physics of Solids. 2020;145:104147.

48. Diebels S, Ehlers W. Dynamic analysis of a fully staturated porous medium accounting for geometrical and material non-linearities. International Journal for Numerical Methods in Engineering. 1996;39:81-97.

49. Zinatbakhsh S, Koch D, Park K, Markert B, Ehlers W. Partitioned formulation and stability analysis of a fluid interacting with a saturated porous medium by localised lagrange mutlipliers. International Journal for Numerical Methods in Engineering. 2016;106:1041-1130.

50. Ghorbani J, Nazem M, Carter J. Numerical modelling of multiphase flow in unsaturated deforming porous media. Computers and Geotechnics. 2016;71:195–206.

51. Klahr B, Medeiros Thiesen J, Teixeira Pinto O, Carniel T, Fancello E. An investigation of coupled solution algorithms for finite-strain poroviscoelasticity applied to soft biological tissues. International Journal for Numerical Methods in Engineering. 2022;123.

52. Navas P, Sanavia L, López-Querol S, Yu R. Explicit meshfree solution for large deformation dynamic problems in saturated porous media. Acta Geotechnica. 2017;13:227-242.

53. Obaid A, Turek S, Heider Y, Markert B. A new monolithic Newton-multigrid-based FEM solution scheme for large strain dynamic poroelasticity problems.

International Journal for Numerical Methods in Engineering. 2017;109:1103–1129.

54. Rohan E, Lukeš V. Modeling large-deforming fluid-saturated porous media using an Eulerian incremental formulation. Advances in Engineering Software. 2017;113:84–95.

55. Vuong AT, Yoshihara L, Wall W. A general approach for modeling interacting flow through porous media under finite deformations. Computer Methods in Applied Mechanics and Engineering. 2015;283:1240–1259.

56. Yuan WH, Zhu JX, Liu K, Zhang W, Dai BB, Wang Y. Dynamic analysis of large deformation problems in saturated porous media by smoothed particle finite element method. Computer Methods in Applied Mechanics and Engineering. 2022;392:114724.

57. Hosseinejad F, Kalateh F, Mojtahedi A. Numerical investigation of liquefaction in earth dams: A comparison of Darcy and non-Darcy flow models. Computers and Geotechnics. 2019;116:103182.

58. Pedroso D. A consistent u-p formulation for porous media with hysteresis. International Journal for Numerical Methods in Engineering. 2015;101:606–634.

59. Salomoni V, Schrefler B. A CBS-type stabilizing algorithm for the consolidation of saturated porous media. International Journal for Numerical Methods in Engineering. 2005;63:502–527.

60. Yoon H, Kim J. Spatial stability for the monolithic and sequential methods with various space discretizations in poroelasticity. International Journal for Numerical Methods in Engineering. 2018;114:694–718.

61. Davison L. Fundamentals of shock wave propagation in solids. Springer; 2008.

62. Clayton J. Nonlinear elastic and inelastic models for shock compression of crystalline solids. Springer; 2019.

63. Simo J, Hughes T. Computational inelasticity. Springer; 1998.

64. Taylor D. Fundamentals of soil mechanics. John Wiley and Sons; 1948.

65. Irwin Z, Regueiro R, Clayton J. A large deformation multiphase continuum mechanics model for shock loading of lung parenchyma. Part II: Numerical methods. DEVCOM Army Research Laboratory (US); 2023. Report No.: ARL-TR-9687.

66. Irwin Z, Regueiro R, Clayton J. A large deformation multiphase continuum mechanics model for shock loading of lung parenchyma. Part III: Numerical simulations. DEVCOM Army Research Laboratory (US); 2023. Report No.: ARL-TR-9688.

67. Hallquist J. LS-DYNA user's manual R12.0. Livermore Software Technology Corporation; 2020.

68. Irwin Z, Clayton J, Regueiro R. A large deformation multiphase continuum mechanics model for shock loading of soft porous materials. International Journal for Numerical Methods in Engineering. Forthcoming 2023.

69. Holzapfel G. Nonlinear solid mechanics: A continuum approach for engineering. John Wiley and Sons; 2000.

70. Clayton J. Nonlinear mechanics of crystals. Springer; 2011.

71. Coleman B, Noll W. The thermodynamics of elastic materials with heat conduction and viscosity. Archive for Rational Mechanics and Analysis. 1963;13:167-178.

72. Ghadiani S. A multiphasic continuum mechanical model for design investigations of an effusion-cooled rocket thrust chamber [thesis]. Institut für Mechanik (Bauwesen) Lehrstuhl für Kontinuumsmechanik; 2005.

73. Markert B. Porous media viscoelasticity with application to polymeric foams [thesis]. Institut für Mechanik (Bauwesen) der Universität Stuttgart; 2005.

74. Marsden J, Hughes T. Mathematical foundations of elasticity. Dover Publications, Inc.; 1983.

75. Truesdell C. Rational thermodynamics. 2nd ed. Springer-Verlag; 1984.

76. Cross J. Mixtures of fluids and isotropic solids. Archive of Mechanics. 1973;6:1025-1039.

77. Clayton J, Freed A. Viscoelastic-damage theory based on a QR decomposition of deformation gradient. DEVCOM Army Research Laboratory (US); 2019. Report No.: ARL-TR-8840.

List of Symbols, Abbreviations, and Acronyms

TERMS:

1-D	one-dimensional
3-D	three-dimensional
ARL	Army Research Laboratory
DEVCOM	US Army Combat Capabilities Development Command
ECM	extra-cellular matrix
f	fluid
FE	finite element
FSI	fluid-structure interaction
ODE	ordinary differential equation
PDE	partial differential equation
RHS	right-hand side
s	solid
TPM	theory of porous media

MATHEMATICAL SYMBOLS:

e	internal energy per unit mass
$\boldsymbol{F}, F_{iJ}$	deformation gradient
p	Cauchy pressure
t	time
$\boldsymbol{u}, u_k$	displacement
V	volume
$\boldsymbol{x}, x_k$	Cartesian spatial coordinates
$\boldsymbol{X}, X_K$	Cartesian reference coordinates
η	entropy per unit mass
ψ	free energy per unit mass

θ	temperature
ρ	mass density
$\boldsymbol{\sigma}, \sigma_{ij}$	Cauchy stress
$\boldsymbol{v}, v_k$	velocity

1 (PDF)	DEFENSE TECHNICAL INFORMATION CTR DTIC OCA
1 (PDF)	DEVCOM ARL FCDD RLB CI TECH LIB
36 (PDF)	DEVCOM ARL FCDD RLA B R BECKER C HOPPEL P GILLICH A TONGE FCDD RLA HC J CRONE J KNAP FCDD RLA MB G GAZONAS FCDD RLA T B LOVE M FERMEN-COKER S SCHOENFELD FCDD RLA TA S TURNAGE C WILLIAMS FCDD RLA TB S ALEXANDER R BANTON T BAUMER D CASEM J CLAYTON B FAGAN A GOERTZ C HAMPTON R KARGUS M KLEINBERGER D KRAYTERMAN J MCDONALD C MEREDITH T PLAISTED K RAFAELS R REGUEIRO S SATAPATHY T WEERASOORIYA C WEAVER S WOZNIAK T ZHANG FCDD RLA TE J LLOYD T SCHARF FCDD RLA TF J CAZAMIAS